

## Supporting Information

### Ambipolar Pentacyclic Diamides with Excellent Electrochemical and Optoelectronic Properties

Carolina S. Marques<sup>1</sup>, Hugo Cruz<sup>2\*</sup>, Simon E. Lawrence<sup>3</sup>, Sandra Gago<sup>2</sup>, João P. Prates Ramalho<sup>1,4,5</sup>, Luís C. Branco<sup>2</sup>, Anthony J. Burke<sup>1,4\*</sup>

<sup>1</sup>LAQV-REQUIMTE, University of Évora, Rua Romão Ramalho, 59, 7000-671 Évora, Portugal

<sup>2</sup>LAQV-REQUIMTE, Departamento de Química, Faculdade de Ciências e Tecnologia, Universidade Nova de Lisboa, 2829- 516 Caparica, Portugal

<sup>3</sup>School of Chemistry, Analytical and Biological Chemistry Research Facility, Solid State Pharmaceutical Centre, University College Cork, Cork, Ireland

<sup>4</sup>Departamento de Química, School of Science and technology, University of Évora, Institute for Research and Advanced Studies, Rua Romão Ramalho, 59, 7000-671 Évora, Portugal

<sup>5</sup>Laboratório Hercules, University of Évora, Palácio do Vimioso, Largo Marquês de Marialva 8, 7000-809 Évora, Portugal

#### Table of Contents:

1. Compounds Synthesis and Characterization Data	p-s2
2. Putative reaction mechanism for the synthesis of <b>(3)</b>	p-s6
3. Compound characterization (NMR and Mass spec.)	p-s7
4. Additional studies	
4.1. Melting point	p-s12
4.2. Chemical stability	p-s12
4.3. Environmentally stability	p-s18
5. SEM analysis of <b>(3)</b> and <b>(4)</b>	p-s23
6. X-ray crystallographic data	p-s24
7. Cyclic voltammetry studies	p-s26
8. Spectroelectrochemical studies	p-s27
9. Quantum Chemical Calculations	p-s28
10. Hole and electron mobilities	p-s32
11. Calculated absorption data for compounds <b>(3)</b> and <b>(4)</b> and the main-orbitals involved in the transitions	p-s34
12. Electroluminescence studies	p-s39
13. References	p-s44

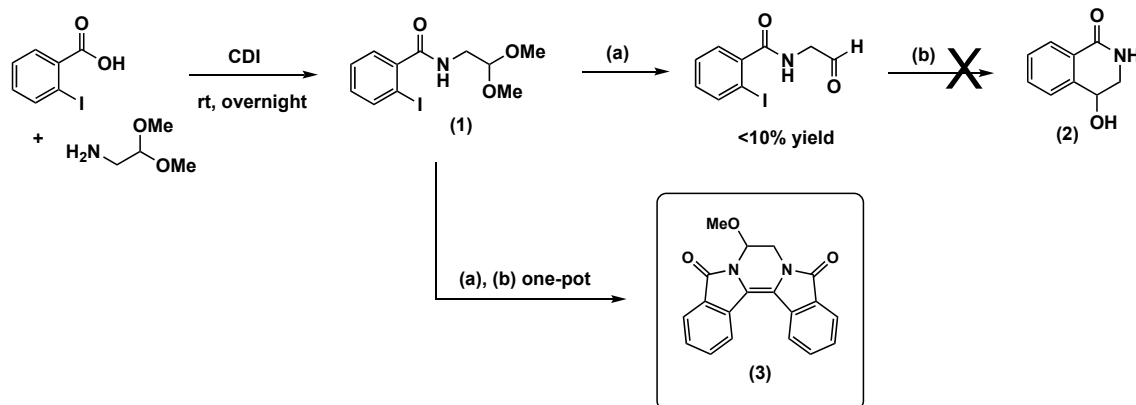
## 1. Compound Synthesis and Characterization data

### General remarks:

All reagents were obtained from Aldrich, Acros and Alfa Aesar and were used as received. When appropriate, the solvents used were dried using current laboratory techniques<sup>1</sup>. All reactions with palladium were conducted under a nitrogen atmosphere. Column chromatography was carried out on silica gel (sds, 70-200 $\mu$ m). Thin layer chromatography (TLC) was carried out on aluminium backed Kieselgel 60 F254 plates (Merck). Plates were visualized either by UV light or with phosphomolybdic acid in ethanol. The NMR analyses were recorded on a Bruker Avance III instrument (400 MHz) and the chemical shifts were quoted in parts per million (ppm) referenced to the appropriate non-deuterated solvent peak relative to 0.0 ppm for tetramethylsilane. Coupling constants (J) are reported in Hz and refer to apparent peak multiplicities. Splitting patterns are reported as s, singlet; d, doublet; t, triplet; dd, doublet of doublets; m, multiplet; br, broad. The mass spectra (MS) were recorded at the University of Vigo on a Bruker FTMS APEXIII instrument using the ESI-TOF technique. X-Ray crystallography was carried out using a Bruker APEX DUO diffractometer using Cu K $\alpha$  radiation ( $\lambda = 1.5418 \text{ \AA}$ ).

UV/Vis absorption spectra were recorded with a Varian Cary 100 Bio spectrophotometer or in a Shimadzu UV-2501-PC and fluorescence spectra were acquired on a SPEX Fluorolog-3 Model FL3-22 spectrofluorimeter. SEM micrographs were obtained using a Phenom ProX instrument (at the University of Evora).

### General Scheme – Synthesis of the pentacyclic diamide (**3**)



**Scheme S1:** Reaction conditions: (a) Acetal deprotection: I<sub>2</sub>, Acetone, reflux, overnight; (b) PdCl<sub>2</sub>(PPh<sub>3</sub>)<sub>2</sub>, Cs<sub>2</sub>CO<sub>3</sub>, THF, 100°C, overnight.

An attempt was made to synthesize the isoquinolinone compound (**2**) via the strategy outlined in Scheme S1. This was to be achieved via deprotection of the acetal (**1a**)<sup>2</sup> followed by a [Pd]-catalysed cyclization onto the carbonyl unit of the intermediate aldehyde to give (**2**). The conditions developed by Hu and co-workers<sup>3</sup> ((a), Scheme S1) gave the corresponding aldehyde in very low yield (<10%). The subsequent cyclization reaction using the coupling conditions reported by Solé and co-workers<sup>4</sup> and by us<sup>2</sup> failed ((b), Scheme S1). As an alternative strategy we decided to carry out the reaction in a sequential one-pot manner. Surprisingly, the pentacyclic diamide

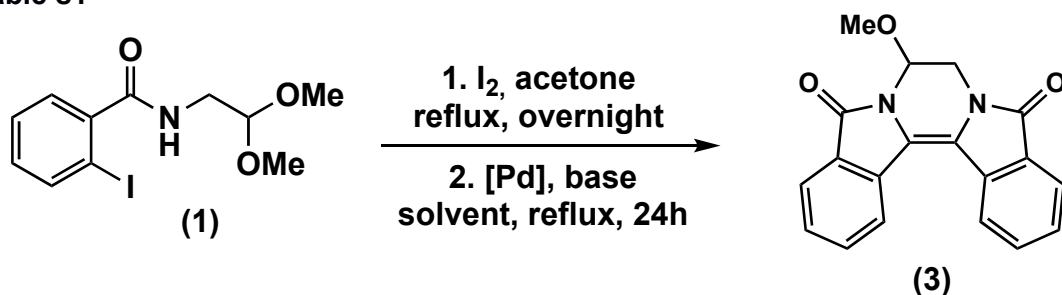
derivative (**3**) was obtained as a fluorescent yellow solid in 16% overall yield (two-steps).

**Synthesis of *N*-(2,2-dimethoxyethyl)-2-iodobenzamide (**1a**)<sup>2</sup>:** 2-Iodobenzoic acid (5.0 g, 0.02 mol), THF (50 mL) and 1,1'-carbonyldiimidazole (3.24 g, 0.02 mol) were added to a round-bottom flask. The mixture was left stirring at room temperature for 30 min. After that, 2,2-dimethoxyethanamine (2.18 mL, 0.02 mol) was slowly added to the reaction flask. The reaction was left stirring at room temperature overnight. The solvent was evaporated under reduced pressure and after purification by column chromatography with SiO<sub>2</sub> gel, using Hexane/ EtOAc (1/1), the *title compound* (**1a**) was obtained as a white oily-solid (6.50 g, 98% yield). <sup>1</sup>H NMR (400 MHz, CDCl<sub>3</sub>) δ: 3.41 (s, 6H, 2×OMe), 3.58 (d, 2H, CH<sub>2</sub>, *J*= 5.2 Hz), 4.53 (t, 1H, CH, *J*= 5.2 Hz), 6.02 (s br, 1H, NH), 7.06-7.10 (m, 1H, Ar), 7.34-7.36 (m, 2H, Ar), 7.83-7.86 (m, 1H, Ar). <sup>13</sup>C NMR (100 MHz, CDCl<sub>3</sub>) δ: 41.3, 53.3, 92.2, 102.0, 128.6, 131.0, 139.1, 143.2, 169.6.

**Synthesis of 4'-hydroxy-4-methoxy-3,4-dihydro-1*H*-2,3'-biisoquinoline-1,1'(2'*H*)-dione (**3**):** A mixture of *N*-(2,2-dimethoxyethyl)-2-iodobenzamide (**1a**) (1 g, 3 mmol), and iodine (76 mg, 0.3 mmol) in acetone (15 ml) was stirred at reflux temperature overnight. Most of the acetone was then removed by evaporation under reduced pressure and the residue was diluted with CH<sub>2</sub>Cl<sub>2</sub> (20 ml). The mixture was washed successively with 5% aq. Na<sub>2</sub>S<sub>2</sub>O<sub>3</sub> (10 ml), H<sub>2</sub>O (20 ml) and *brine* (20 ml). The organic layer was separated, dried over MgSO<sub>4</sub> and filtered. The solvent was removed under reduced pressure. The crude product was passed through a glass column filled with SiO<sub>2</sub> gel and eluted with Et<sub>2</sub>O. The major fraction was recovered and evaporated under reduced pressure to afford the "pre-purified" crude product that was dissolved in dry THF (20 ml). PdCl<sub>2</sub>(PPh<sub>3</sub>)<sub>2</sub> (0.18 g, 20 mol%) and Cs<sub>2</sub>CO<sub>3</sub> (1.3 g, 3 equiv.) were then added to the reaction flask, under an inert atmosphere. The reaction was stirred at 100°C for 18 hours. The solvent was evaporated under reduced pressure and the crude product dissolved in CH<sub>2</sub>Cl<sub>2</sub> (20 ml) and washed with aq. sat. NaHCO<sub>3</sub> (20 ml), H<sub>2</sub>O (20 ml) and *brine* (20 ml). The organic phase was dried with MgSO<sub>4</sub>, filtered and evaporated under reduced pressure. The crude product was purified by silica gel column chromatography using heptane/Et<sub>2</sub>O (1:1) as eluent to afford the *title compound* (**3**) as a yellow solid (0.078 g, 16% from two-steps). <sup>1</sup>H NMR (CDCl<sub>3</sub>, 400 MHz) δ: 3.42 (s, 3H, OCH<sub>3</sub>), 3.53 (dd, *J*= 16 Hz, 1H, CH<sub>2</sub>), 4.74 (dd, *J*= 16 Hz, 1H, CH<sub>2</sub>), 5.93-5.94 (m, 1H, CH), 7.52-7.59 (m, 2H, Ar), 7.68-7.76 (m, 2H, Ar), 7.95 (d, *J*= 8 Hz, 1H, Ar), 8.01 (d, *J*= 8 Hz, 1H, Ar), 8.20-8.26 (m, 2H, Ar). <sup>13</sup>C NMR (CDCl<sub>3</sub>, 100 MHz) δ: 42.7, 56.9, 75.6, 117.8, 120.9, 122.7, 124.6, 125.1, 129.1, 129.4, 130.2, 132.6, 132.9, 133.5, 165.2, 165.4. **HR-MS (ESI) m/z** Calcd for C<sub>19</sub>H<sub>15</sub>N<sub>2</sub>O<sub>3</sub> ((M<sup>+</sup>)-H<sub>2</sub>O) 319.10827, Found 319.10772 ((M<sup>+</sup>)-H<sub>2</sub>O) for C<sub>19</sub>H<sub>15</sub>N<sub>2</sub>O<sub>3</sub>.

Reaction Screening:

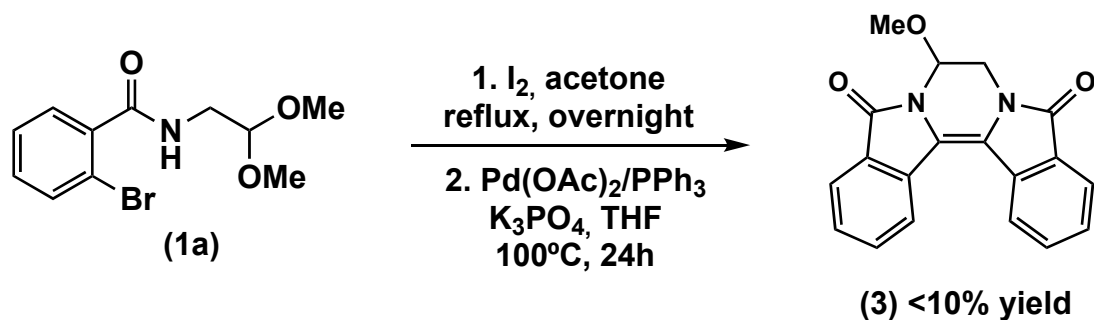
Table s1



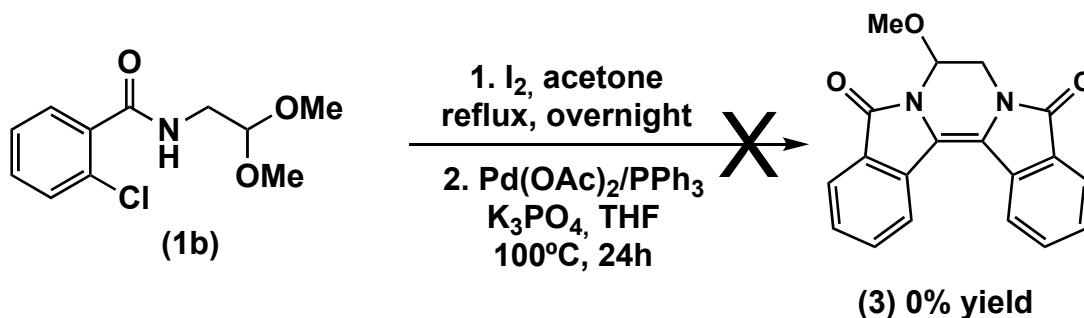
Entry	[Pd] <sup>a</sup>	Base <sup>b</sup>	Solvent	Temp./°C	Yield/% (2 steps)
1	PdCl <sub>2</sub> (PPh <sub>3</sub> ) <sub>2</sub>	Cs <sub>2</sub> CO <sub>3</sub>	THF	100	16
2	PdCl <sub>2</sub> (dppf)	Cs <sub>2</sub> CO <sub>3</sub>	THF	100	11
3	PdCl <sub>2</sub> (CH <sub>3</sub> CN)	Cs <sub>2</sub> CO <sub>3</sub>	THF	100	0
4	Pd(CH <sub>3</sub> CN) <sub>4</sub> (BF <sub>4</sub> ) <sub>2</sub>	Cs <sub>2</sub> CO <sub>3</sub>	THF	100	0
5	Pd(OAc) <sub>2</sub> /PPh <sub>3</sub>	Cs <sub>2</sub> CO <sub>3</sub>	THF	100	13
6	Pd(dba) <sub>2</sub> /PPh <sub>3</sub>	Cs <sub>2</sub> CO <sub>3</sub>	THF	100	13
7	Pd(OAc) <sub>2</sub> /PPh <sub>3</sub>	K <sub>2</sub> CO <sub>3</sub>	THF	100	<10
8	Pd(OAc) <sub>2</sub> /PPh <sub>3</sub>	KOtBu	THF	100	0
9	Pd(OAc) <sub>2</sub> /PPh <sub>3</sub>	KOAc	THF	100	0
10	Pd(OAc) <sub>2</sub> /PPh <sub>3</sub>	NEt <sub>3</sub>	THF	100	17
11	Pd(OAc) <sub>2</sub> /PPh <sub>3</sub>	K <sub>3</sub> PO <sub>4</sub>	THF	100	18
12	PdCl <sub>2</sub> (PPh <sub>3</sub> ) <sub>2</sub>	K <sub>3</sub> PO <sub>4</sub>	THF	100	17
13	Pd(OAc) <sub>2</sub> /PPh <sub>3</sub>	DIPEA	THF	100	12
14	Pd(OAc) <sub>2</sub> /PPh <sub>3</sub>	Na <sub>2</sub> CO <sub>3</sub>	THF	100	0
15	-	K <sub>3</sub> PO <sub>4</sub>	THF	100	0
16	Pd(OAc) <sub>2</sub> /PPh <sub>3</sub>	-	THF	100	0
17	Pd(OAc) <sub>2</sub> /PPh <sub>3</sub>	K <sub>3</sub> PO <sub>4</sub>	CH <sub>3</sub> CN	100	<10
18	Pd(OAc) <sub>2</sub> /PPh <sub>3</sub>	K <sub>3</sub> PO <sub>4</sub>	MeTHF	100	<10
19	Pd(OAc) <sub>2</sub> /PPh <sub>3</sub>	K <sub>3</sub> PO <sub>4</sub>	DME	100	11
20	Pd(OAc) <sub>2</sub> /PPh <sub>3</sub>	K <sub>3</sub> PO <sub>4</sub>	DCE	100	<5
21	Pd(OAc) <sub>2</sub> /PPh <sub>3</sub>	K <sub>3</sub> PO <sub>4</sub>	Dioxane	120	14
22	Pd(OAc) <sub>2</sub> /PPh <sub>3</sub>	K <sub>3</sub> PO <sub>4</sub>	Toluene	120	<10

<sup>a</sup>20 mol%. <sup>b</sup>3 equivalents.

Other acetal-derivatives:



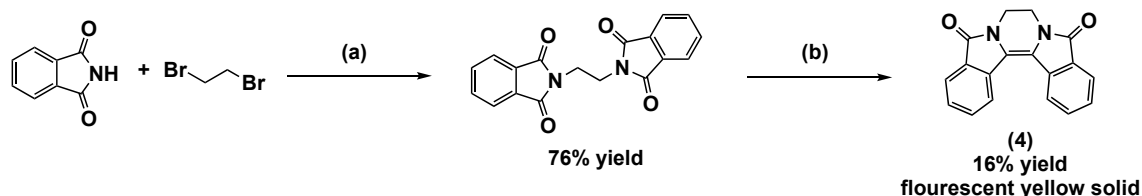
The synthesis of acetal derivative **2-bromo-*N*-(2,2-dimethoxyethyl)benzamide (1b)** was achieved using a similar procedure as that described above for **(1a)**, but starting with 2-bromobenzoic acid. **(1a)** was obtained in 90% yield as a white solid.  $^1\text{H NMR}$  (400 MHz,  $\text{CDCl}_3$ )  $\delta$ : 3.40 (s, 6H, 2 $\times$ OMe), 3.56-3.58 (t, 2H,  $\text{CH}_2$ ,  $J = 4$  Hz), 4.49-4.51 (t, 1H, CH,  $J = 4$  Hz), 6.25 (s br, 1H, NH), 7.22-7.25 (m, 1H, Ar), 7.31-7.34 (m, 1H, Ar), 7.47-7.50 (m, 1H, Ar), 7.55-7.57 (d, 1H, Ar,  $J = 8$  Hz).  $^{13}\text{C NMR}$  (100 MHz,  $\text{CDCl}_3$ )  $\delta$ : 41.5, 54.5, 102.5, 119.3, 127.6, 129.6, 131.4, 133.4, 137.8, 167.8.



The synthesis of acetal derivative **2-chloro-*N*-(2,2-dimethoxyethyl)benzamide (1c)** was achieved using similar procedure applied for **(1a)** using 2-chlorobenzoic acid. A white solid of **(1b)** was obtained in 95% yield.  $^1\text{H NMR}$  (400 MHz,  $\text{CDCl}_3$ )  $\delta$ : 3.38 (s, 6H, 2 $\times$ OMe), 3.53-3.56 (m, 2H,  $\text{CH}_2$ ), 4.46-4.49 (m, 1H, CH), 6.50 (s br, 1H, NH), 7.24-7.36 (m, 3H, Ar), 7.55-7.57 (d, 1H, Ar,  $J = 8$  Hz).  $^{13}\text{C NMR}$  (100 MHz,  $\text{CDCl}_3$ )  $\delta$ : 41.5, 54.4, 102.5, 127.0, 129.9, 130.2, 130.7, 131.3, 135.0, 166.7.

#### General Scheme – Synthesis of the pentacyclic diamide **(4)**

Compound **(4)** already exists in literature<sup>5</sup>, but here we describe a new synthetic approach to its synthesis:

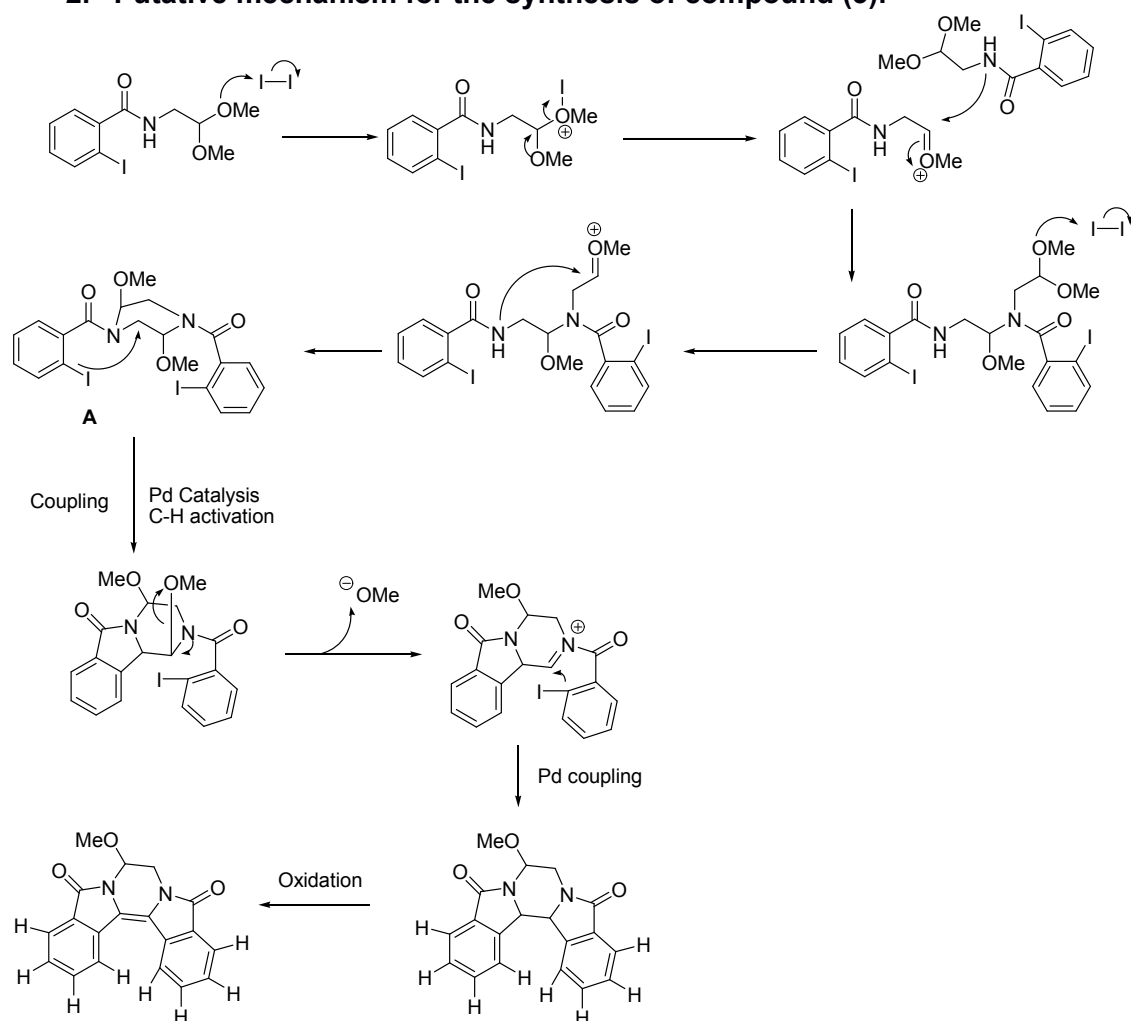


**Scheme s2:** Reaction conditions: (a) TBAB (cat),  $\text{K}_2\text{CO}_3$ , DMF,  $40^\circ\text{C}$ , 2 days; (b) McMurry coupling reaction:  $\text{TiCl}_4$ , Zn, Py, THF,  $0^\circ\text{C}$  to reflux, overnight.

**Synthesis of 2,2'-(ethane-1,2-diyl)bis(isoindoline-1,3-dione)**<sup>6</sup>: A mixture of phthalimide (1 g, 6.8 mmol), 1,2-dibromoethane (0.3 mL, 3.4 mmol),  $\text{K}_2\text{CO}_3$  (1.9 g, 13.6 mmol), tetrabutylammonium bromide (TBAB, 219 mg, 0.68 mmol) and DMF (15 mL) was left stirring at  $40^\circ\text{C}$  during 24 hours. After that a second addition of phthalimide (0.5 g) was made into the reaction flask and the mixture left stirring at  $40^\circ\text{C}$  for more 24 hours. Next the mixture was cooled to room temperature and then poured into water (50 mL) and the product extracted with AcOEt (5 $\times$ 50 mL). The combined organic phases were dried with  $\text{MgSO}_4$ , filtered and the solvent evaporated under reduced pressure. The crude product 2,2'-(ethane-1,2-diyl)bis(isoindoline-1,3-dione) was obtained as a white solid (0.82 g, 76% yield) and using without additional purification.  $^1\text{H NMR}$  (400 MHz,  $\text{DMSO-}d_6$ )  $\delta$ : 3.84 (s, 4H,  $\text{CH}_2$ ), 7.81 (s, 8H, Ar).  $^{13}\text{C NMR}$  (100 MHz,  $\text{DMSO-}d_6$ )  $\delta$ : 36.32, 123.12, 131.35, 134.53, 167.80.

**Synthesis of 7,8-dihydropyrazino[2,1-a:3,4-a']diisoindole-5,10-dione<sup>7</sup>:** Under an inert atmosphere, a two neck flask equipped with a magnetic stirrer was charged with Zn powder (1.6 g, 24 mmol) and THF (40 mL). The mixture was cooled to 0 °C and TiCl<sub>4</sub> (1.3 mL, 12 mmol) was slowly added by syringe. The suspending mixture was warmed to room temperature and stirred for half an hour, then heated at reflux for 3 h. The mixture was again cooled to 0 °C, charged with pyridine (0.5 mL, 6 mmol) and stirred during 10 min. The 2,2'-(ethane-1,2-diyl)bis(isoindoline-1,3-dione) (0.78 g, 2.4 mmol) in THF (15 mL) was added slowly to reaction mixture. After addition the reaction mixture was heated at reflux temperature overnight and monitored by TLC. The reaction was quenched with 10% aq. K<sub>2</sub>CO<sub>3</sub> and extracted with CH<sub>2</sub>Cl<sub>2</sub>. The organic layer was collected and concentrated under reduced pressure. The crude product was purified by silica gel flash chromatography using CHCl<sub>3</sub>/AcOEt (1/1) and AcOEt as eluents. The corresponding 7,8-dihydropyrazino[2,1-a:3,4-a']diisoindole-5,10-dione<sup>5</sup> (0.11 g, 16% yield) was obtained as a yellow solid. <sup>1</sup>H NMR (400 MHz, DMSO-*d*<sub>6</sub>) δ: 4.02 (s, 4H, CH<sub>2</sub>), 7.61-7.65 (t, *J* = 8 Hz, 2H, Ar), 7.78-7.82 (t, *J* = 8 Hz, 2H, Ar), 7.88-7.90 (d, *J* = 8 Hz, 2H, Ar), 8.35-8.37 (d, *J* = 8 Hz, 2H, Ar). <sup>13</sup>C NMR (100 MHz, DMSO-*d*<sub>6</sub>) δ: 37.09, 119.91, 123.05, 123.68, 129.29, 129.41, 132.65, 132.79, 163.78. HR-MS (ESI) *m/z* Calcd for C<sub>18</sub>H<sub>12</sub>N<sub>2</sub>O<sub>2</sub> 288.0898, Found 289.0972 (M<sup>+</sup>) for C<sub>18</sub>H<sub>13</sub>N<sub>2</sub>O<sub>2</sub>.

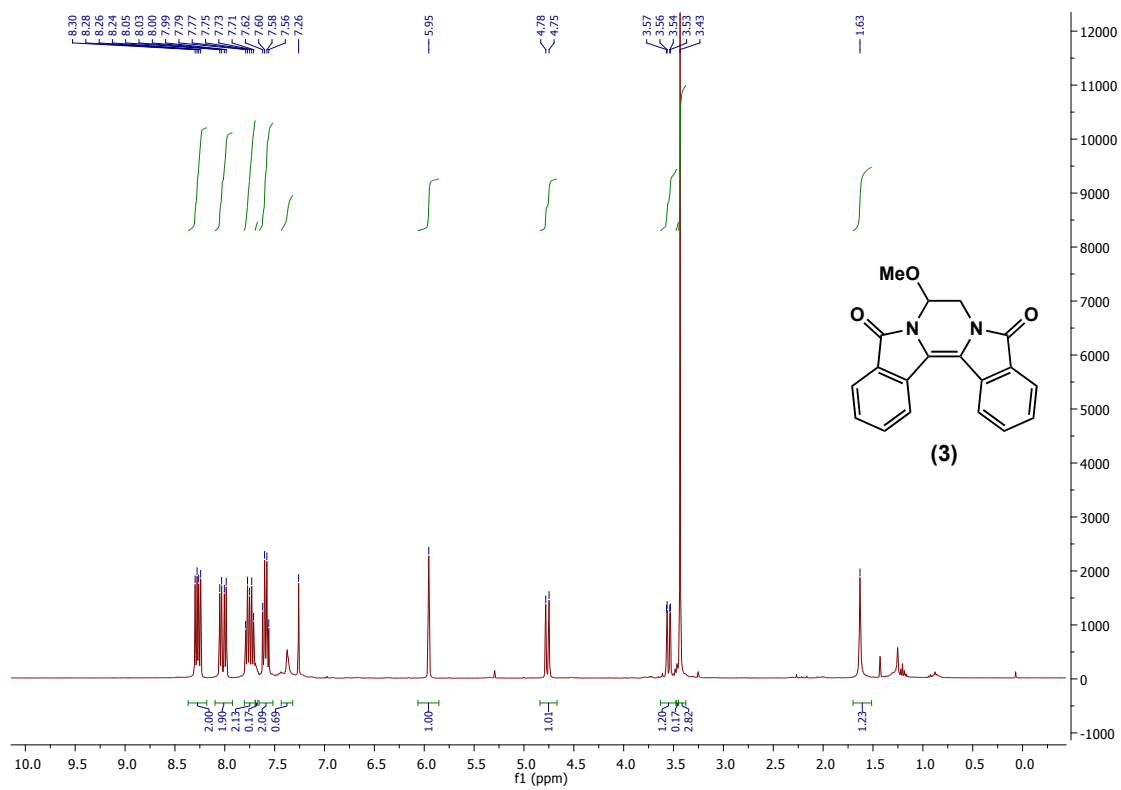
## 2. Putative mechanism for the synthesis of compound (3).



**Scheme s3:** Putative mechanism for the synthesis of compound (3).

### 3. Spectral Characterization data for compounds (3) and (4)

<sup>1</sup>H and <sup>13</sup>C NMR:





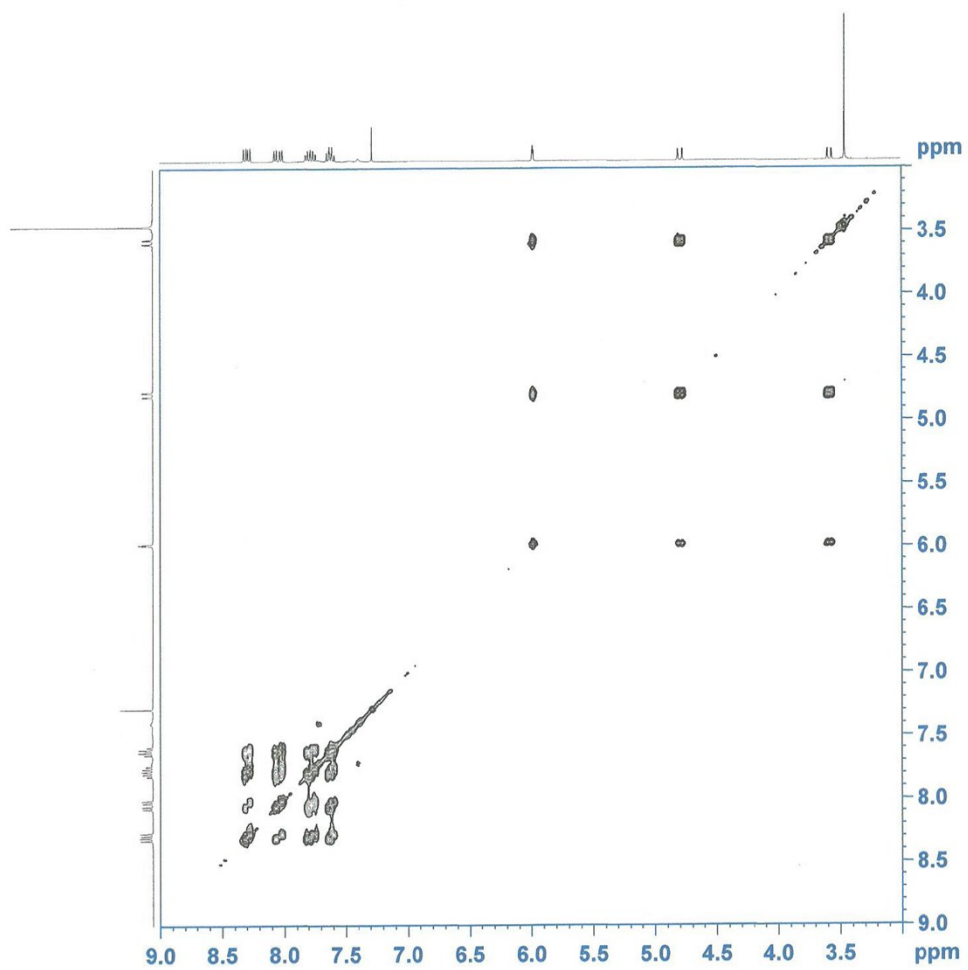


Fig. s2 COSY (<sup>1</sup>H-<sup>1</sup>H) (CDCl<sub>3</sub>, 400 MHz) of (3)

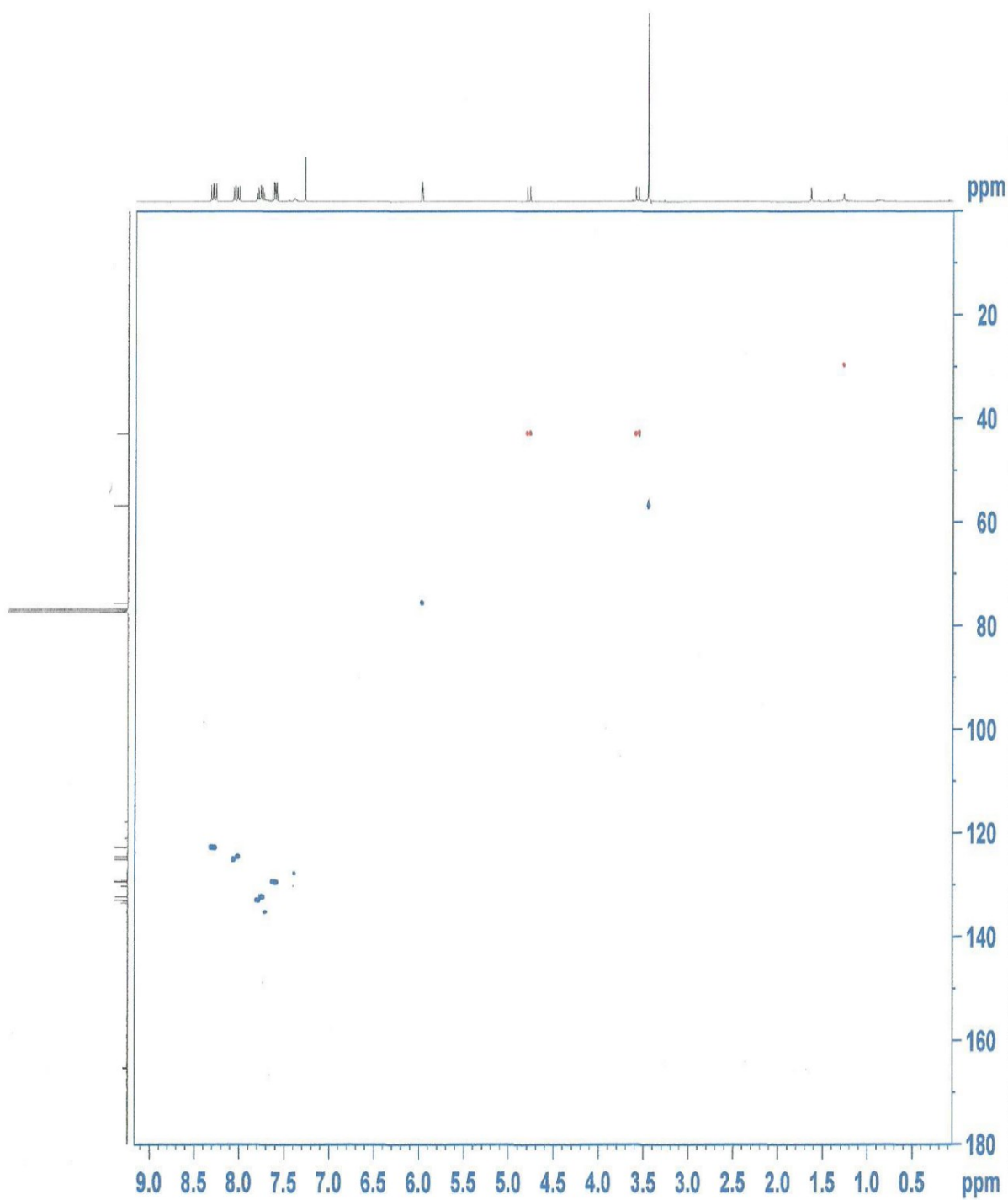


Fig. s3 HSQC (CDCl<sub>3</sub>, 400 MHz) spectrum of (3)

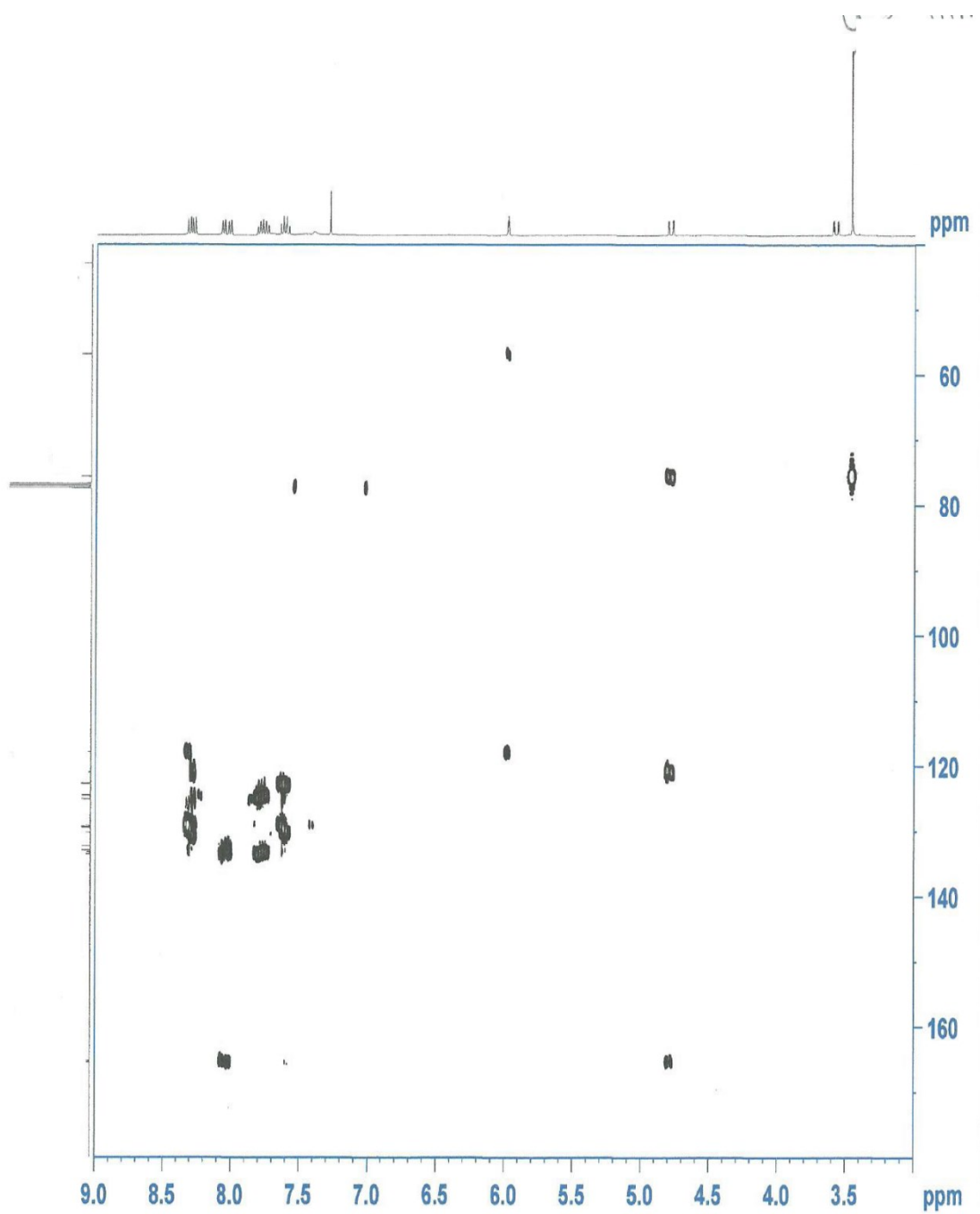
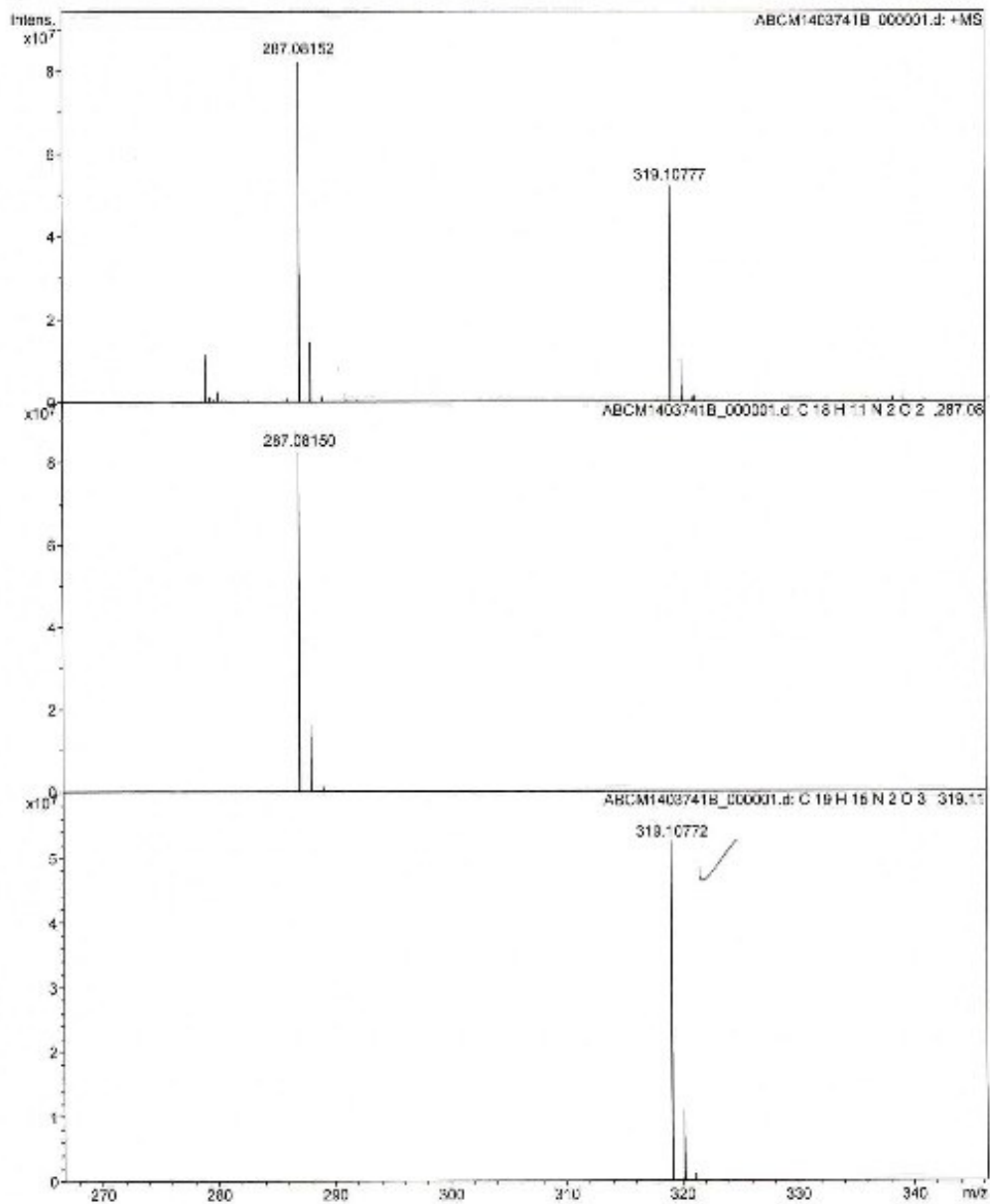


Fig. s4 HMQC ( $\text{CDCl}_3$ , 400 MHz) spectrum of (3)

### Mass Spectrum Molecular Formula Report

Analysis Info                      Electrospray (ESI)  
Analysis Name    ABCM1403741B\_000001.d                      Acquisition Date    n/a  
Sample Name                      Uc659                      Instrument            apex-Qe



U.Vigo/CACTI/DEPyG/Apex-Qe

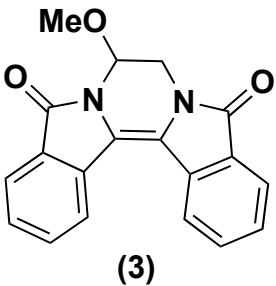
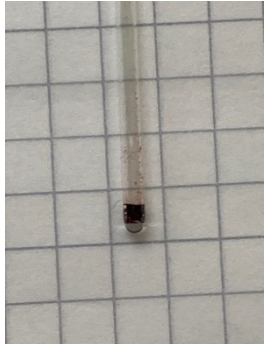
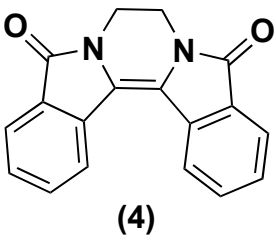
Page 1 of 2

Fig. s5 HRMS of (3)

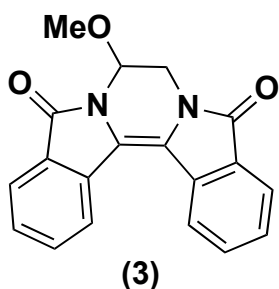
#### 4. Additional studies:

##### 4.1. Melting point (vaporability studies)

Table s2

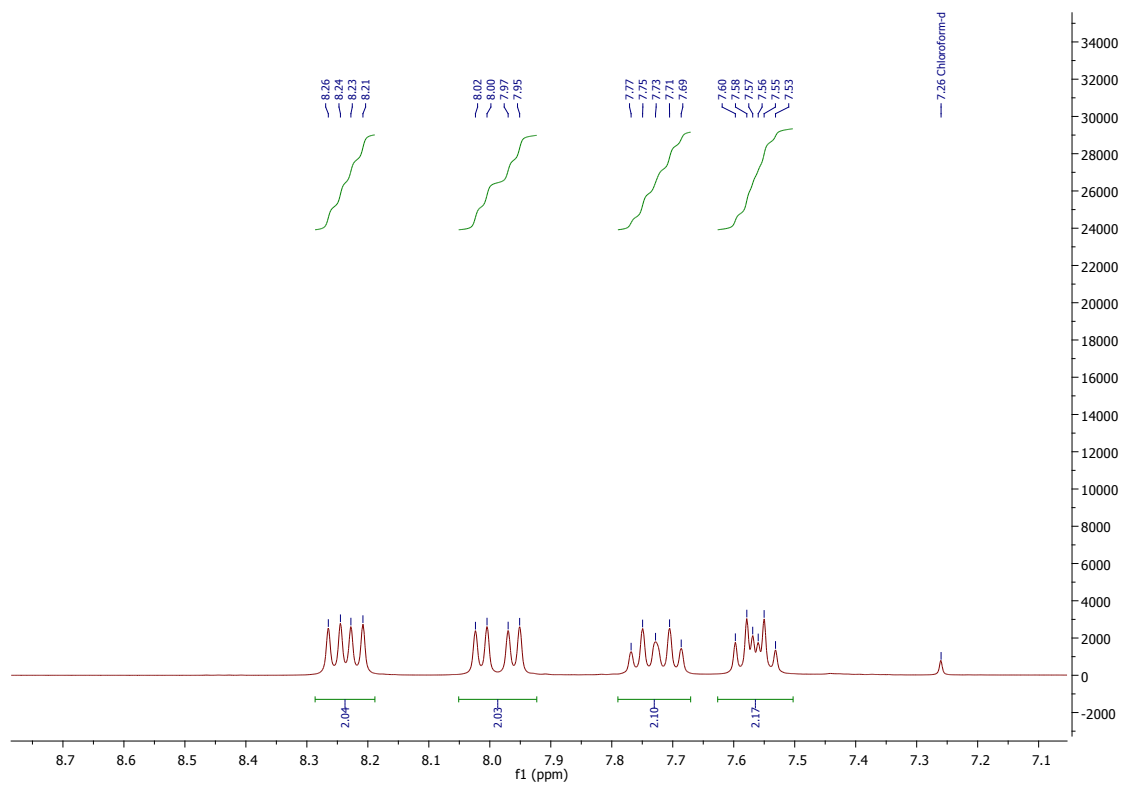
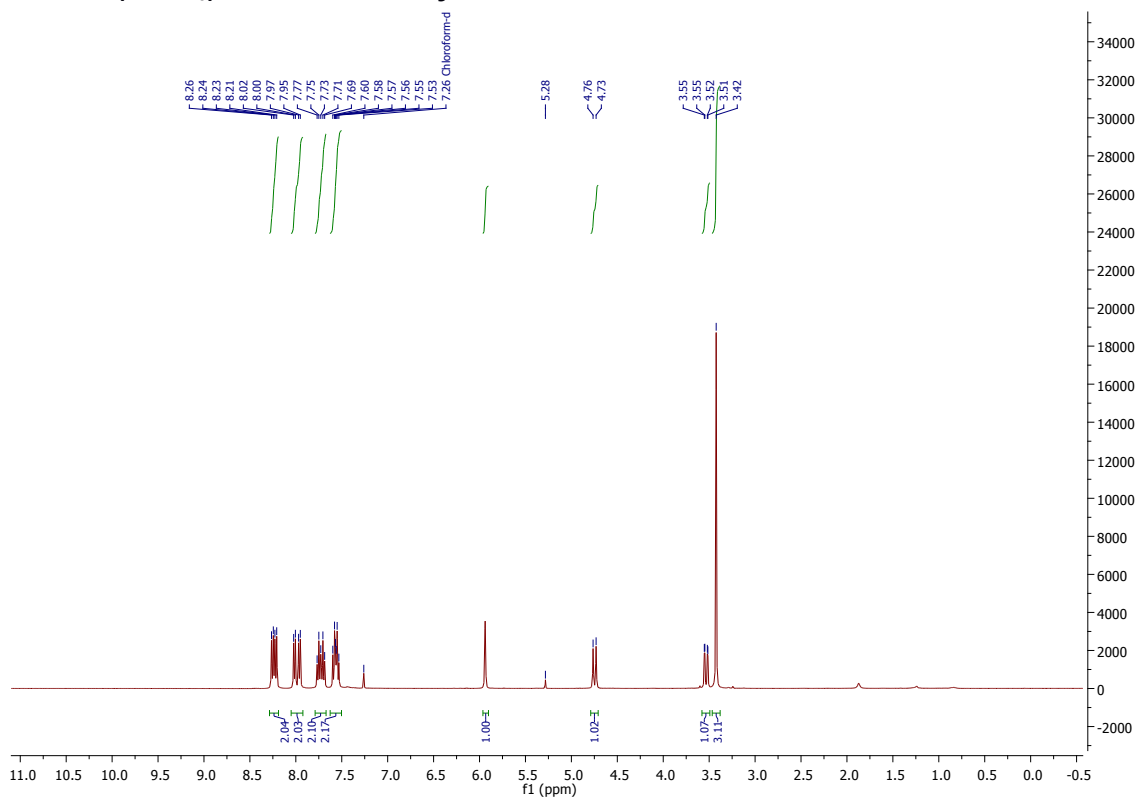
Compound	Observations	
 (3)	rt: Yellow solid; 195°C: sample starts to change color - yellow to orange to dark orange; 220°C: sample became darker but still solid; 226°C: starts melting; 227.5°C: completely melted but very dark;	
 (4)	rt: yellow solid; 202°C: sample starts to change color – yellow to dark yellow; 214.5°C: dark yellow to brown; 244.5°C: dark brown – no melting; >280°C: sample becomes black – without melting;	

##### 4.2. Chemical Stability



In a round-bottomed flask fitted with a water condenser, 33.9 mg of compound (3) was stirred with 7 mL of toluene at 120°C, for 16 hours. After that the solvent was evaporated the resulting compound was analyzed by <sup>1</sup>H NMR . The spectra of compound (3) before and after heating can be seen below. There were no alterations in the compound colour.

**<sup>1</sup>H NMR (CDCl<sub>3</sub>) before the study:**



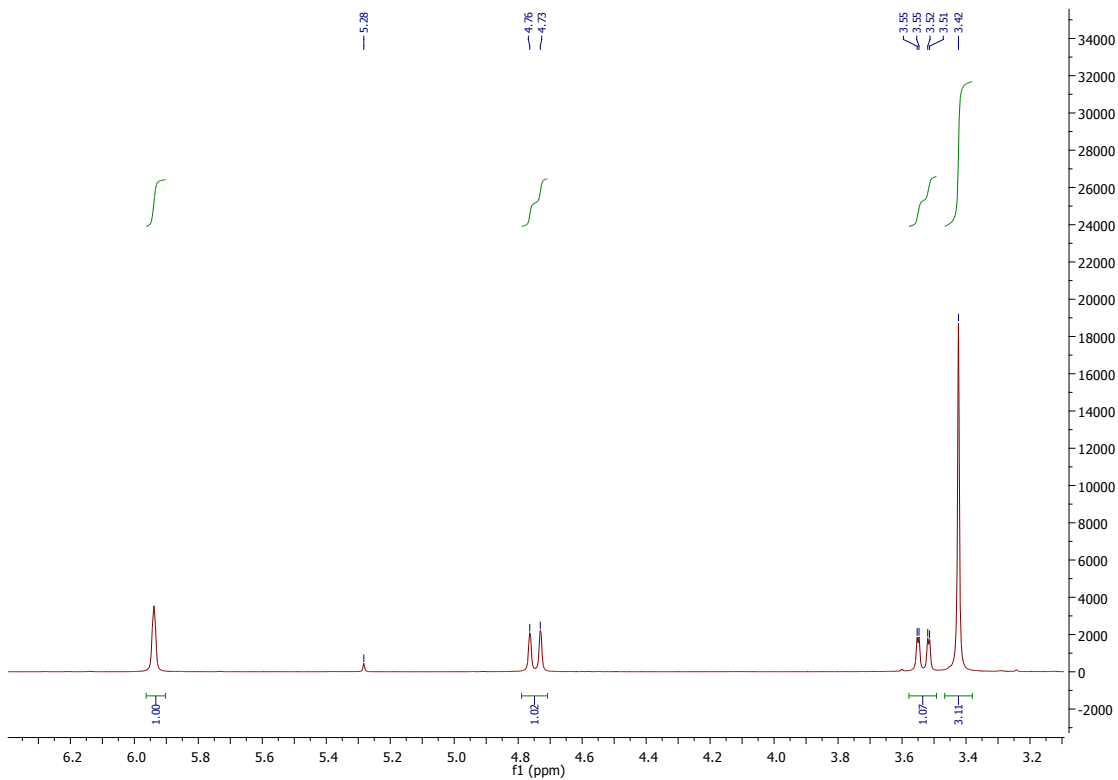
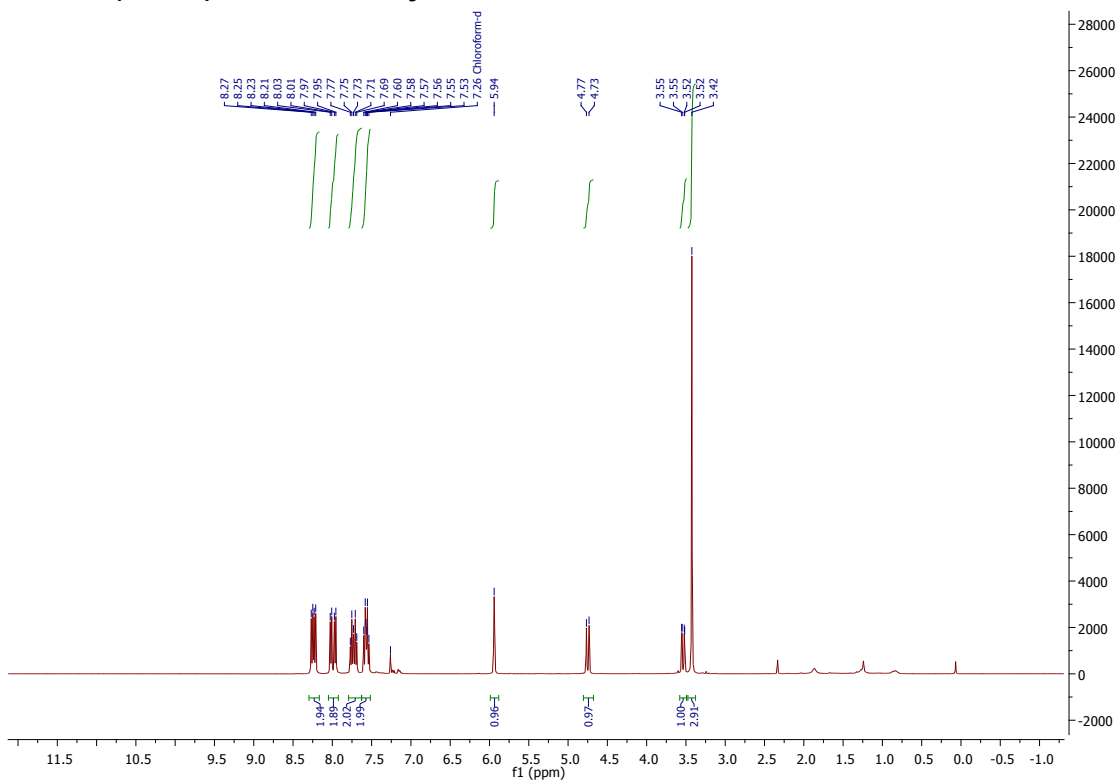


Fig. s6

$^1\text{H}$  NMR ( $\text{CDCl}_3$ ) after the study:



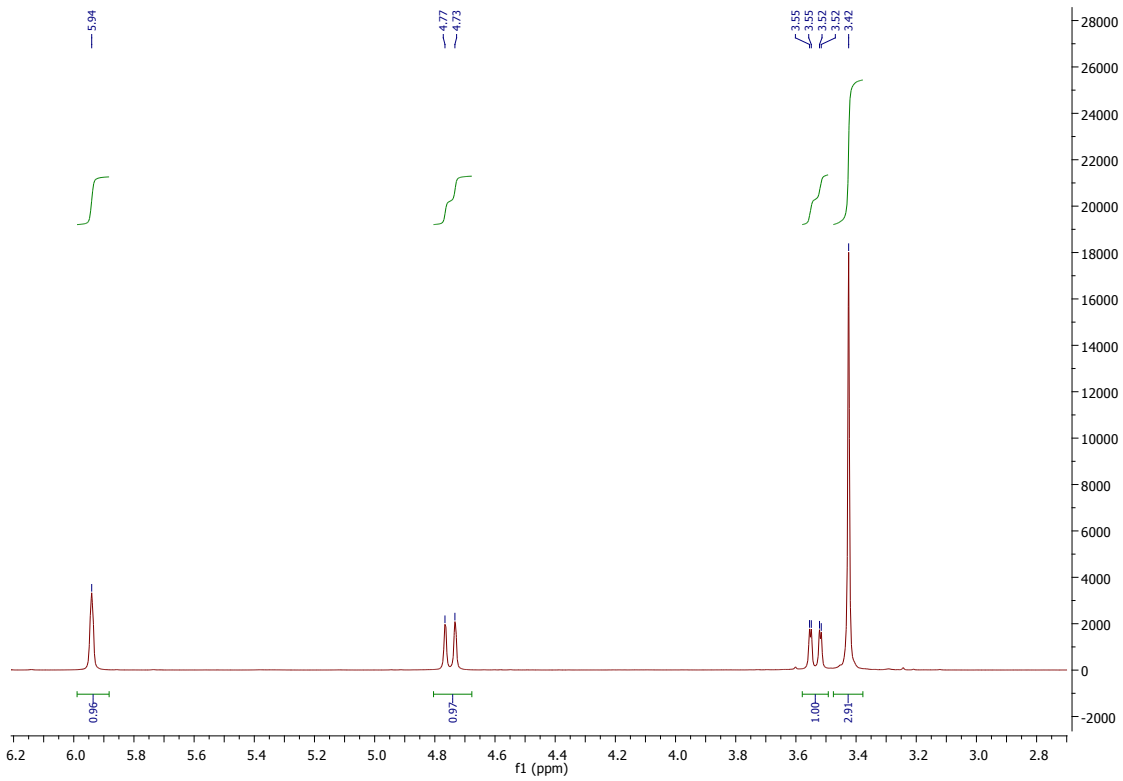
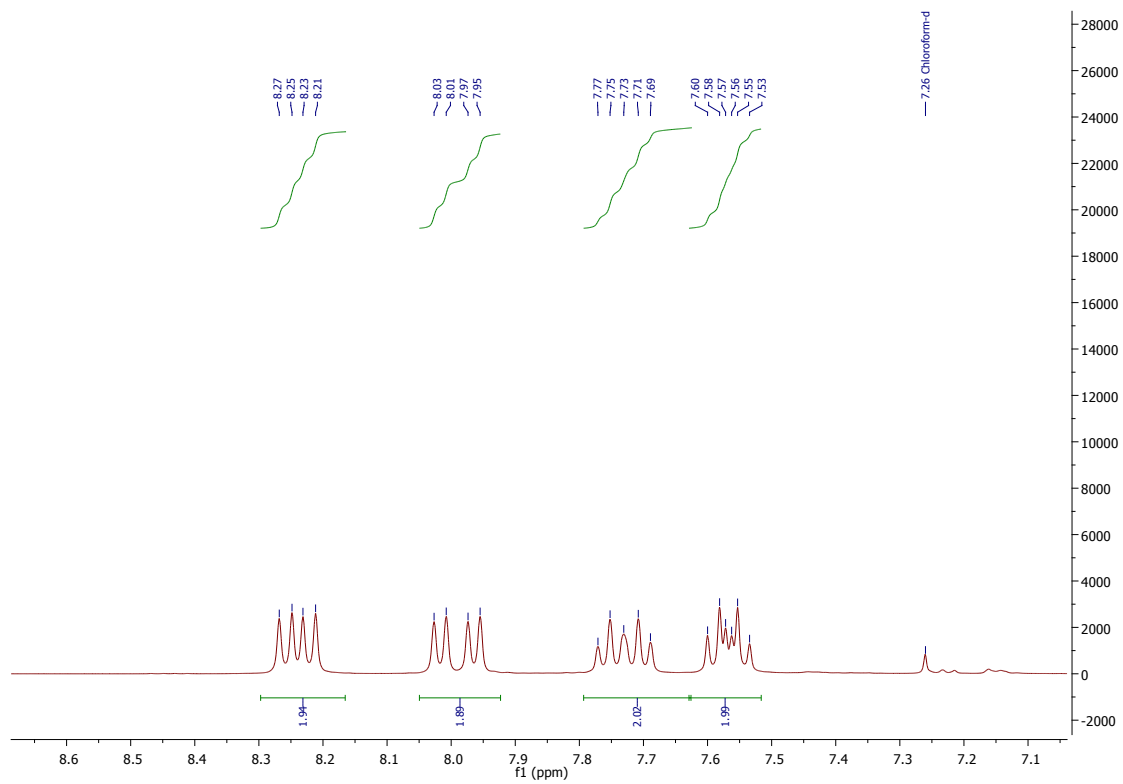
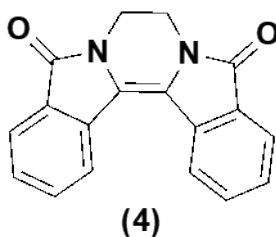
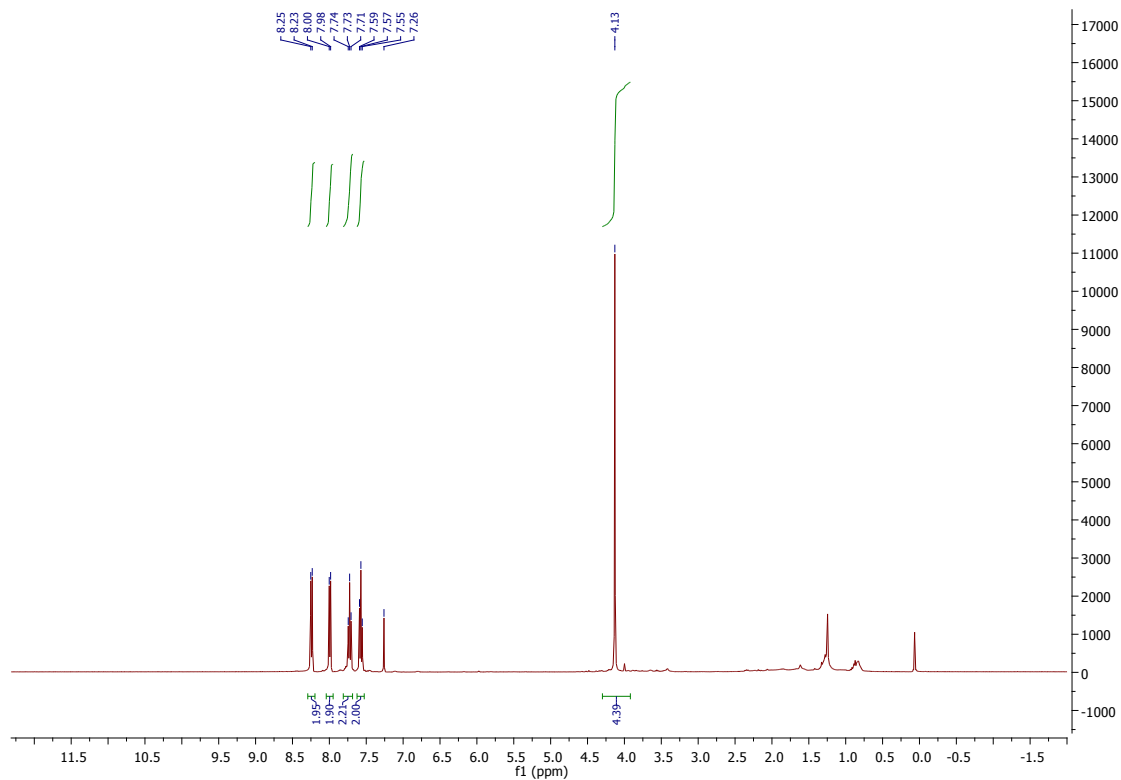


Fig. s7



In a round-bottomed flask fitted with a water condenser, 14.7 mg of compound (4) was stirred with toluene (5 mL) at 120°C, for 15 hours. The solvent was evaporated and the compound analyzed by  $^1\text{H}$  NMR. The spectra of the compound (4) before and after heating are seen below. There were no alterations in colour.

$^1\text{H}$  NMR ( $\text{CDCl}_3$ ) before the study:



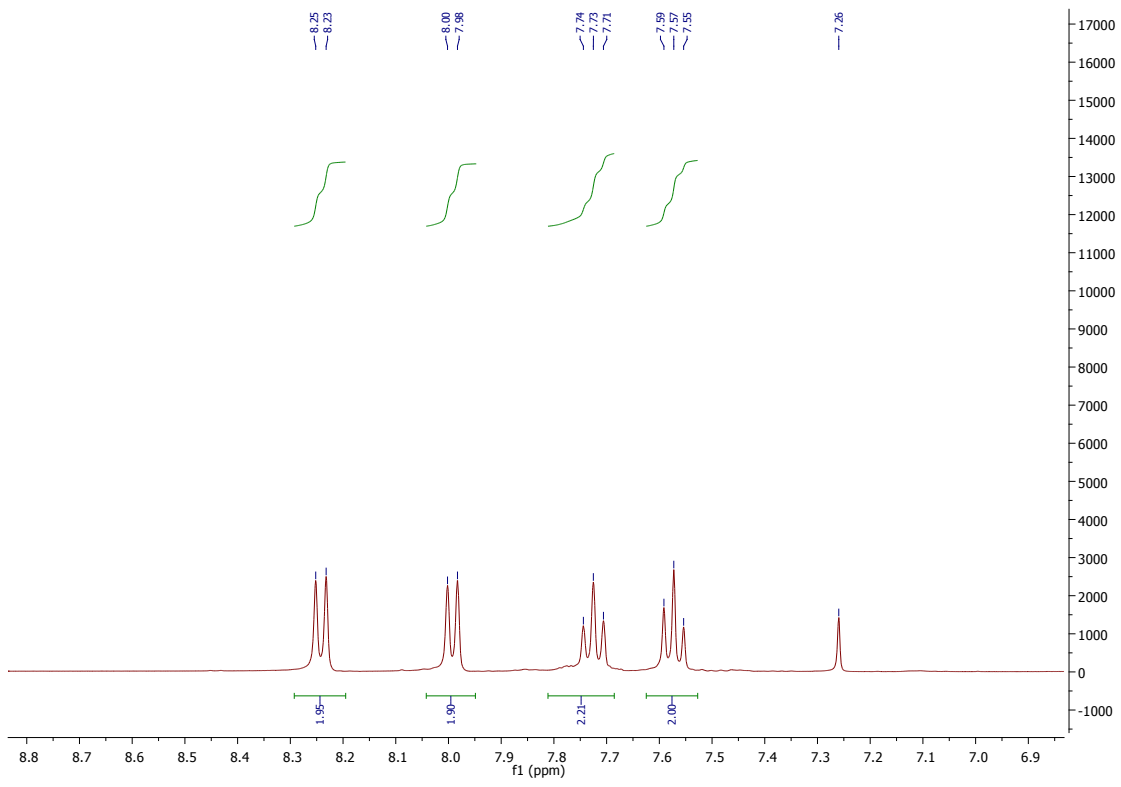
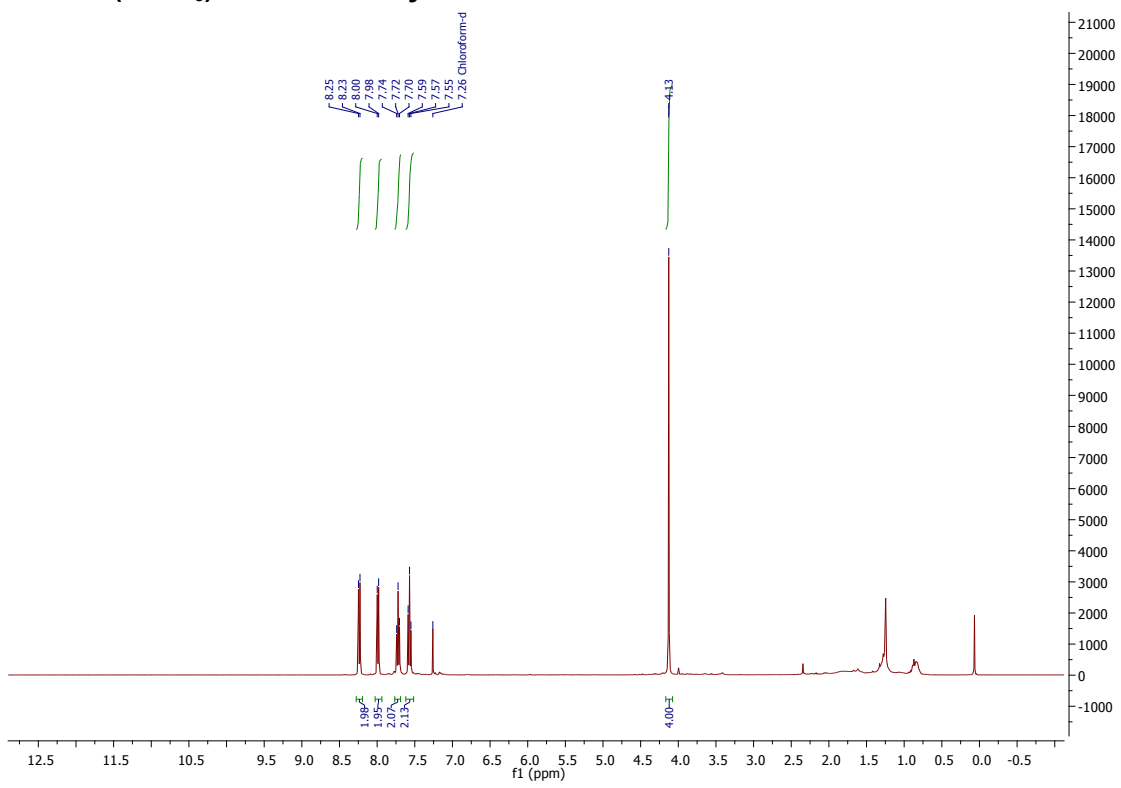
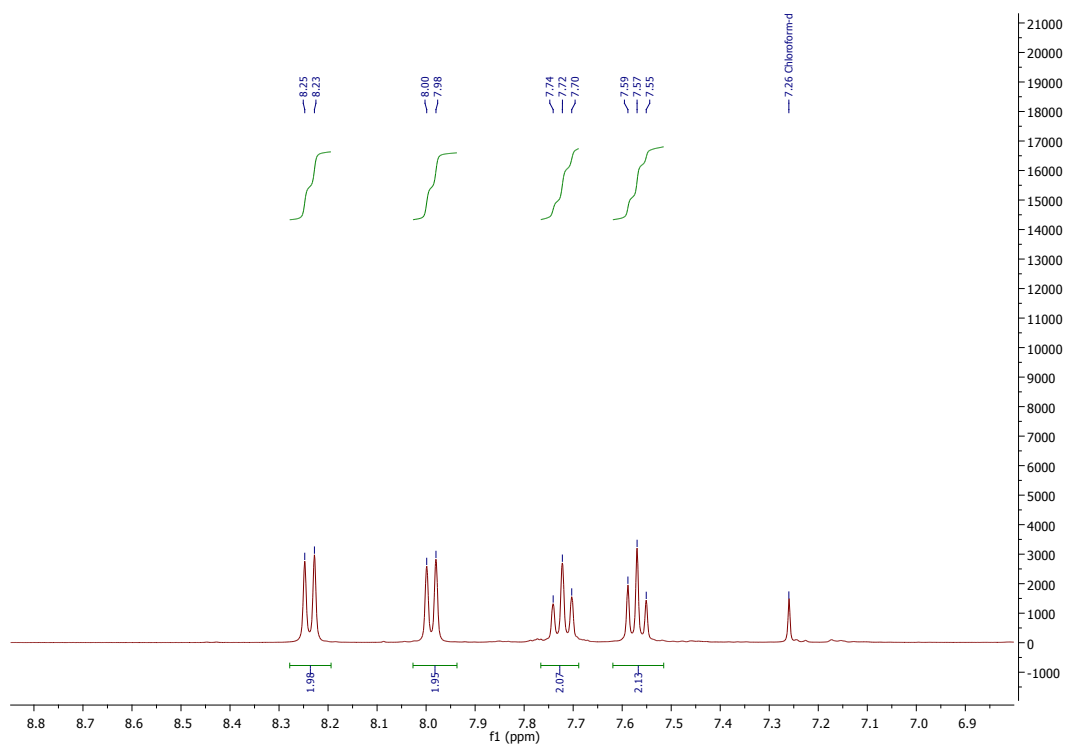


Fig. s8

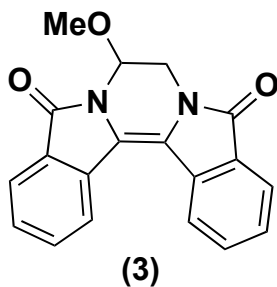
1H NMR (CDCl<sub>3</sub>) after the study:





**Fig. s9**

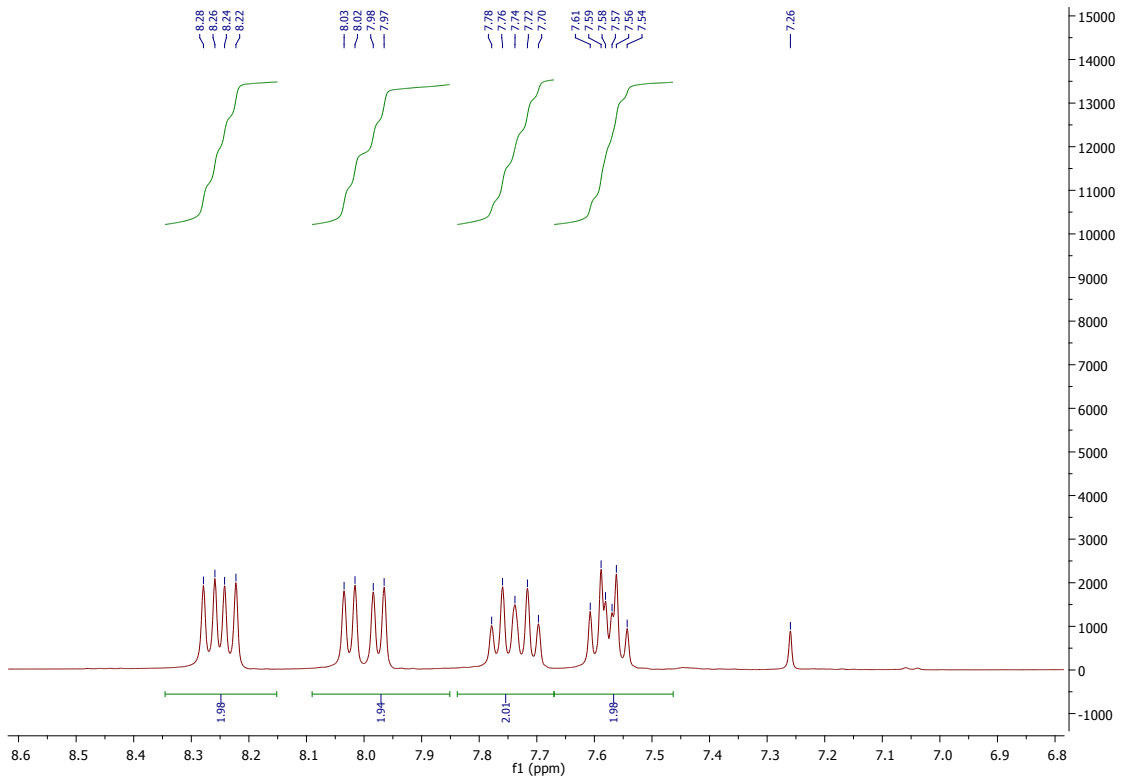
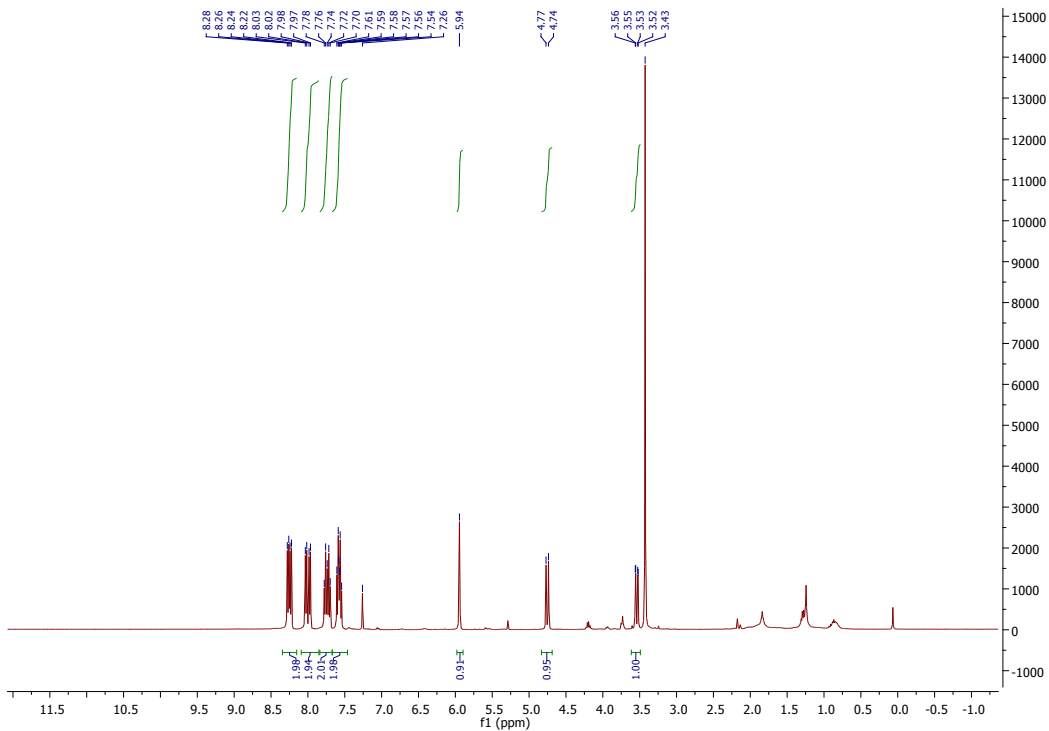
### 4.3. Environmentally Stability (stability in aqueous mixtures)



In a round-bottomed flask, 26.4 mg of compound **(3)** was stirred at room temperature with THF (5 mL) and water (5 mL) for 20 hours. After that DCM (3x20 mL) was added to the reaction mixture and extraction of the organic phase was made. The combined organic phases were dried with MgSO<sub>4</sub>, filtered and the solvent evaporated under reduced pressure. The compound was analyzed by <sup>1</sup>H NMR in CDCl<sub>3</sub>. The spectra can be seen below.

No alterations in the compound color were observed.

**<sup>1</sup>H NMR (CDCl<sub>3</sub>) after the study:**



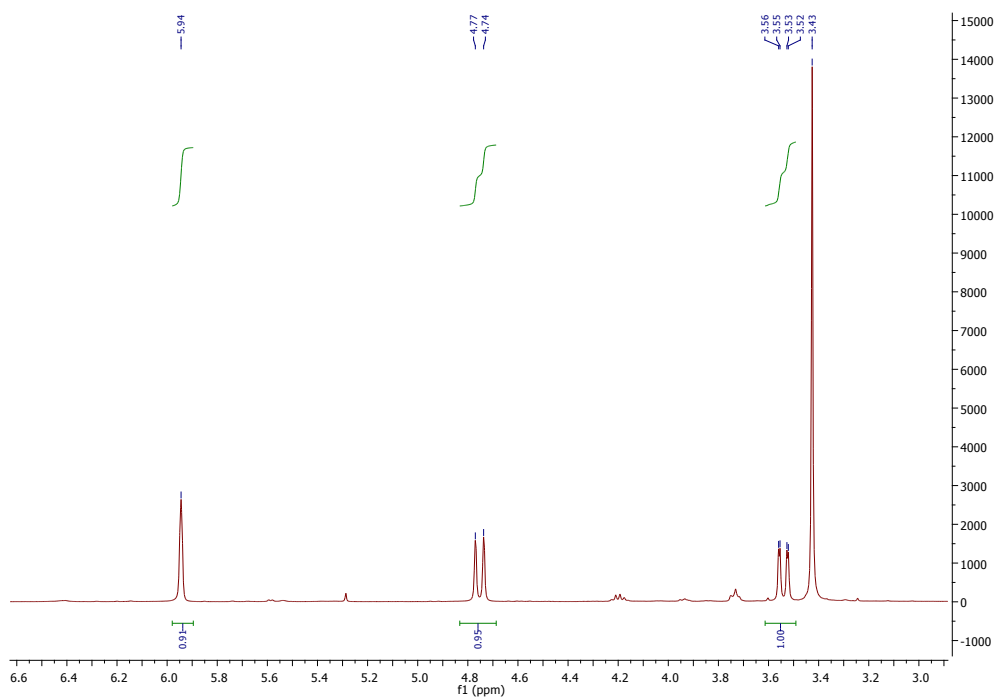
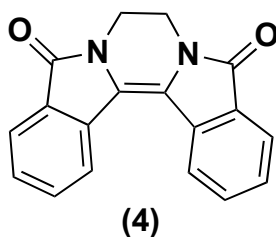


**Fig. s10**



In a round-bottomed flask, 14.2 mg of compound **(4)** was stirred at room temperature with THF (5mL) and water (5mL) for 20 hours. After that DCM (3x20 mL) was added to the reaction mixture and extraction of the organic phase was made. The combined organic phases were dried with  $\text{MgSO}_4$ , filtered and the solvent evaporated under reduced pressure. The compound was analyzed by  $^1\text{H}$  NMR. The spectra can be seen in Fig. s11. There were no alterations in the compound color.

**<sup>1</sup>H NMR (CDCl<sub>3</sub>) after the study:**

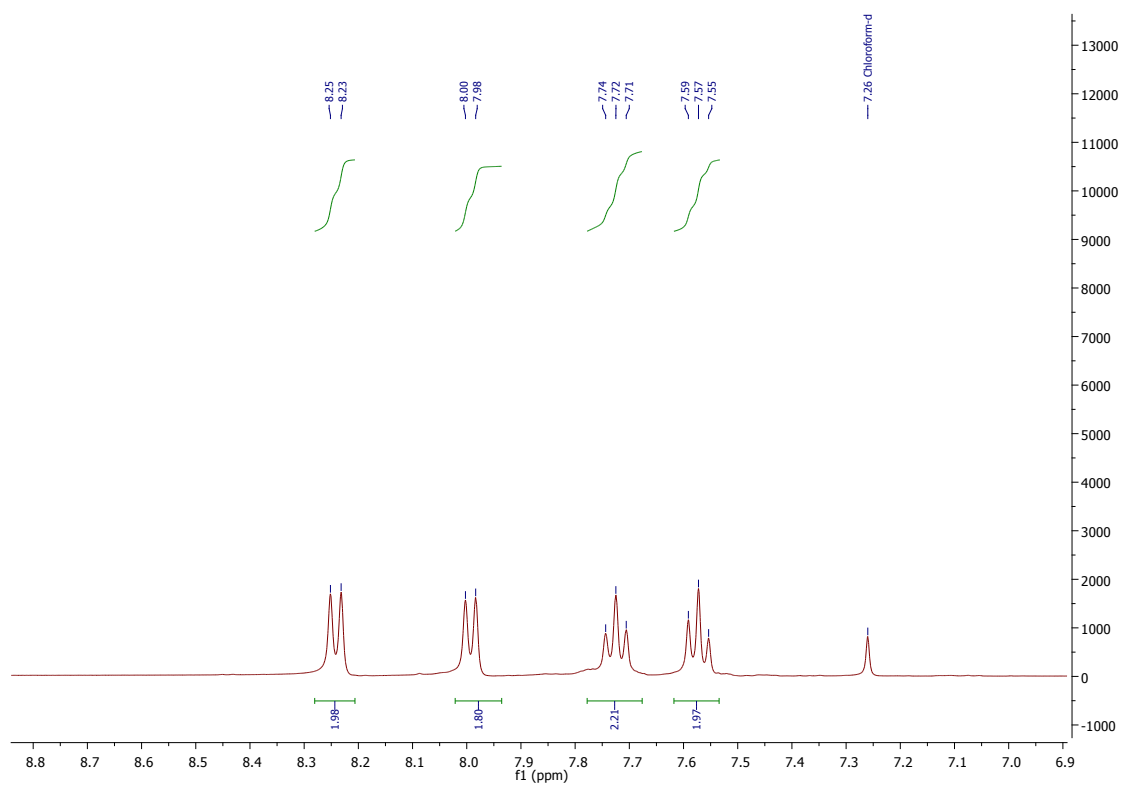
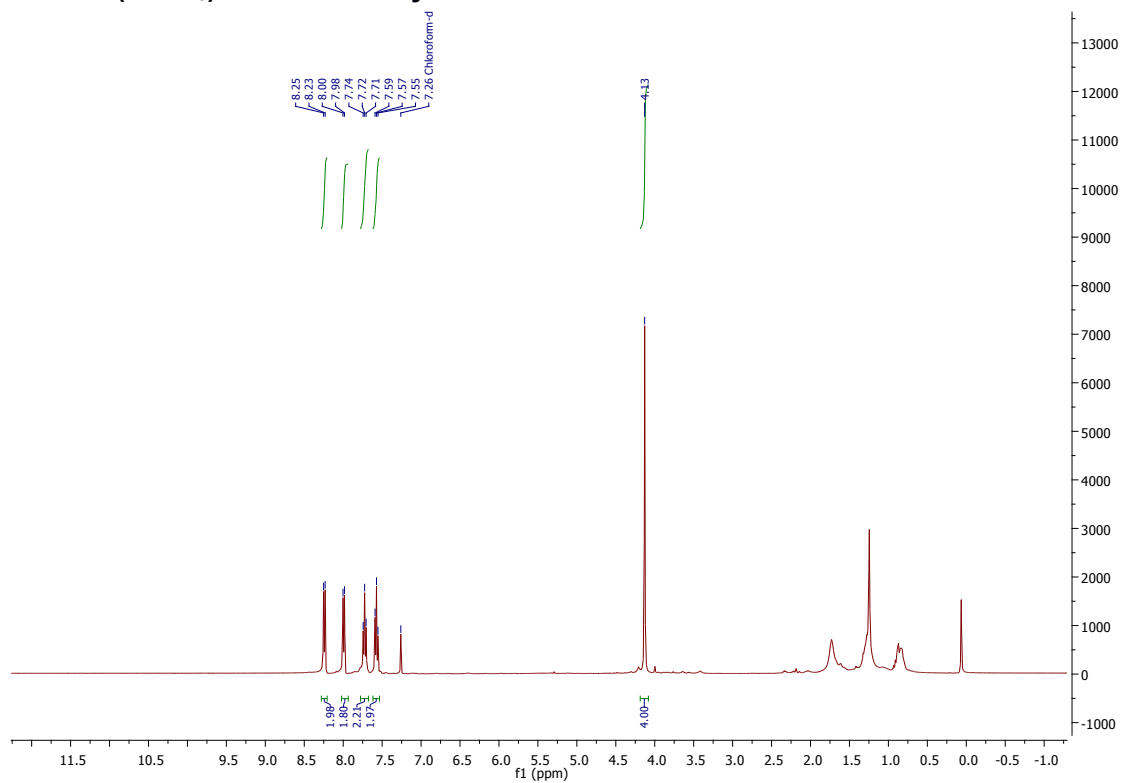
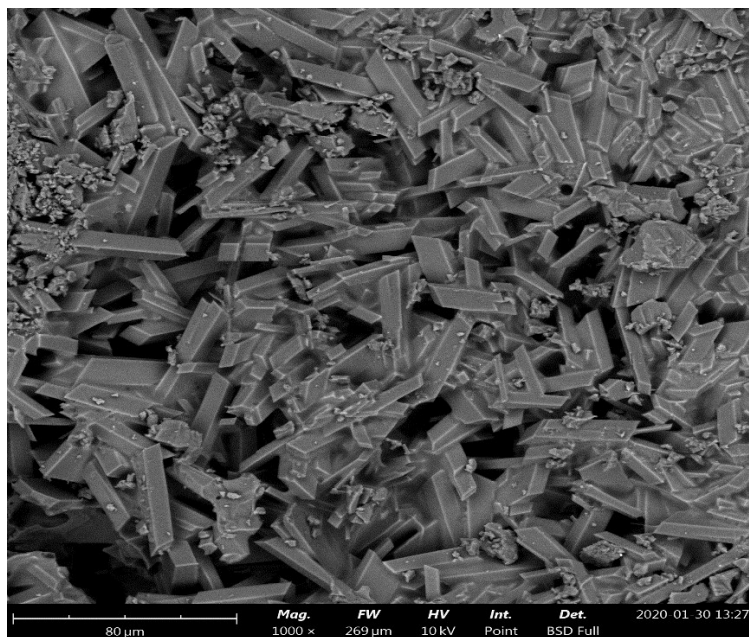


**Fig. s11**

## 5. Scanning Electron Microscopy

(a)



(b)

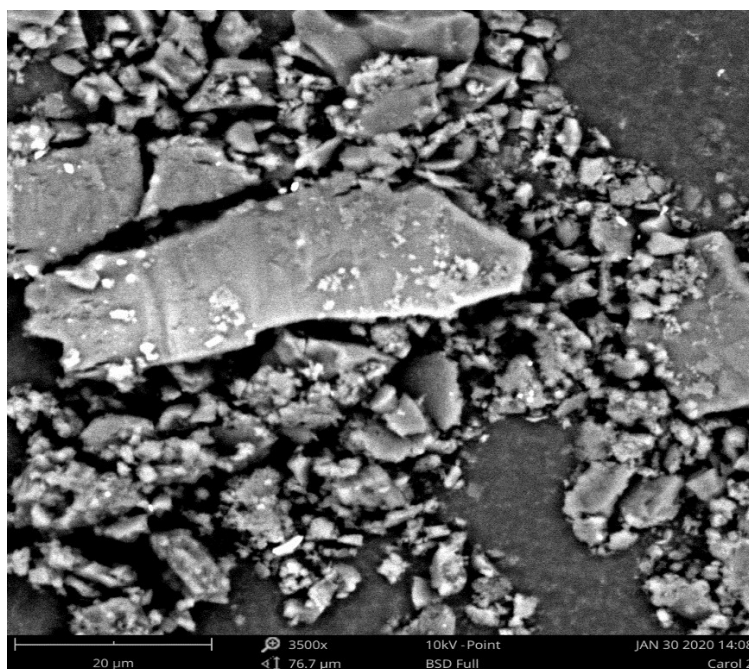


**Figure s12** Micrographs obtained by SEM: (a) shows compound (3) and (b) shows compound (4).

## 6. X-ray crystallographic Studies

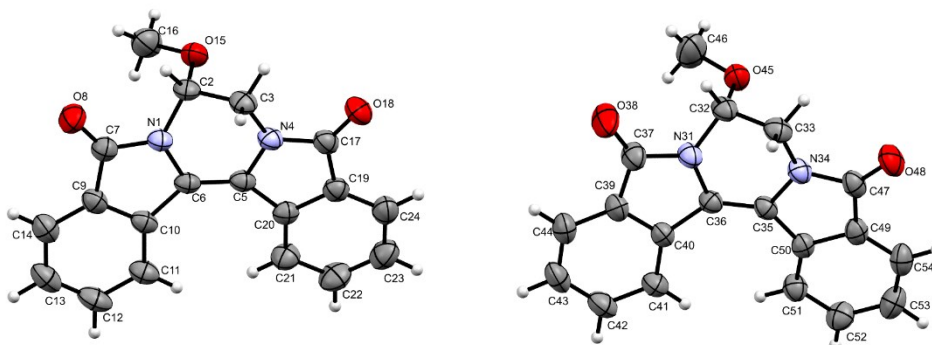


**Figure s13** ORTEP plots of the two crystallography independent molecules in **(3)**. Anisotropic displacement parameters are drawn at the 50% probability level.

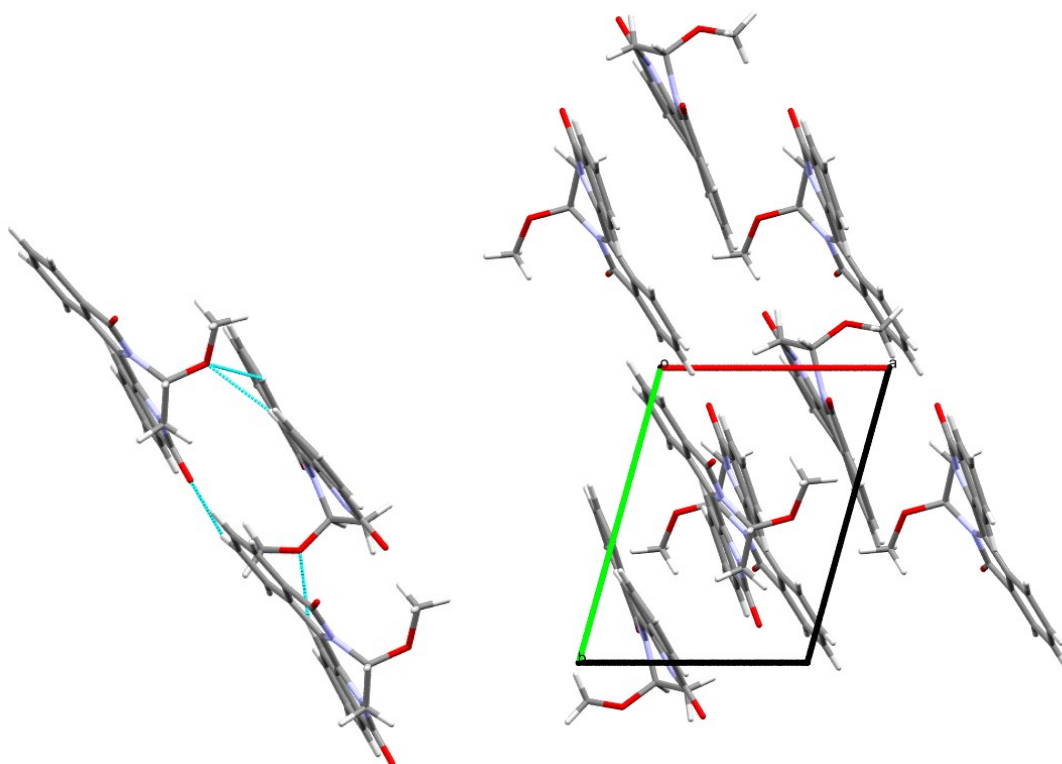


**Figure s14** The C-H...O hydrogen bonding seen in **(3)** (left) and packing showing the *ab* plane (right).

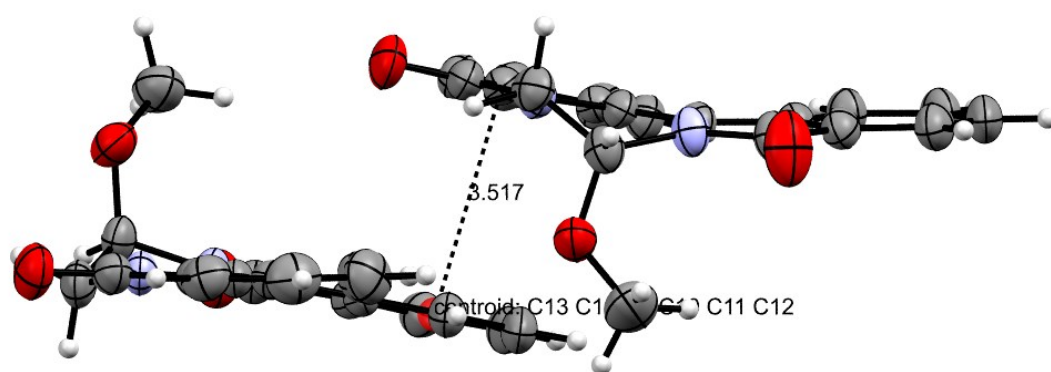


**Figure s15** Image showing one possible pi...pi interaction (from a carbon on a ring to the centroid of a neighbouring phenyl ring).

## 7. Cyclic voltammetry studies

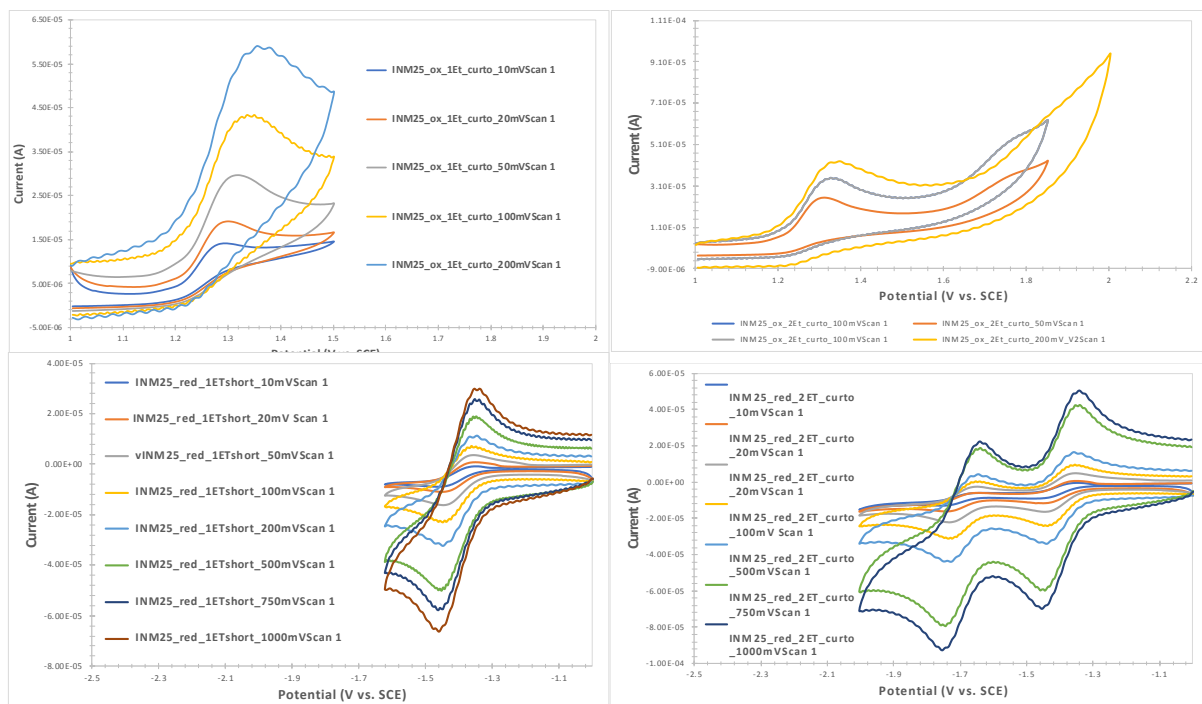
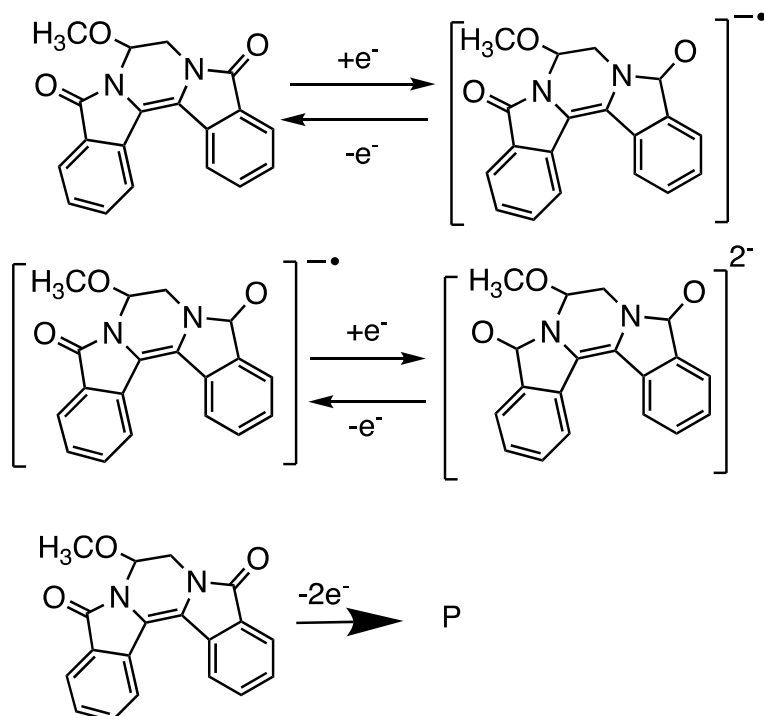


**Figure s.16.** Electrochemical study of compound (3). Prepared as a solution of 1mM of (3) with 0.1M TBAP in acetonitrile at different scan rates. A) direct anodic scan for the 1<sup>st</sup> oxidation of the material; b) direct anodic scan for the 1<sup>st</sup> and 2<sup>nd</sup> oxidations of the material; c) direct cathodic scan for the 1<sup>st</sup> reduction of the material; d) direct cathodic scan for the 1<sup>st</sup> and 2<sup>nd</sup> reduction of the material.

Reduction in anhydride media



**Scheme s4:** Putative redox mechanism for the reduction of **(3)** under anhydrous conditions.

## 8. Spectroelectrochemical studies.

An anodic electrochemical process was performed by applying +1.5V (vs. SCE). The dicationic species from compound **(3)** were also investigated by cyclic voltammetry (CV), electrolysis and spectroelectrochemistry experiments. The initial spectrum of **(3)** consisted of two major absorption bands at 280nm and a broad band at 325-450 nm. During the scan period of 3600s and just after the 210s mark, these spectra changed and the intensity of the broad band (325-450 nm) started to decrease whilst the band at 250nm increased with concomitant discoloration of the sample at the end of the scan. It appears that the cationic radical and charged species play a critical role on the charge carriers of the semiconducting heteroatom-doped **(3)** associated with the doped state. From the chemical irreversible two-electron oxidation waves observed from the CV study, it was suggested that the dipositive charged species are not stable under the measurement conditions. However, this study indicates that the dicationic species obtained from **(3)** is unstable, leading to the formation of an unknown chemical entity **(P)** (see Fig. s4 and Fig. s5) after the oxidation process. We also believe that in this process **(3)** suffers loss of aromaticity of the molecule. In this study, the following was observed: upon initiation of the oxidation process (the cell presents a yellow coloration) the coloration becomes darker as the potential is increased from 0V to 1.25V vs. SCE and when the potential was just over 1.35V the sample became brown, this coloration was reversible in that when the electrolysis was terminated the coloration returned to the original yellow color. In order to obtain the product **(P)** the sample was removed during the electrolysis but it appeared that not all the product was formed and this would explain the reversion to the original yellow coloration.

The reduction of the sample at -1.5V (vs. SCE) was also performed and at -1.5V the Pt grid becomes blue then it became green after mixing the sample. Two samples were recovered one at the electrolysis time and other after applying a potential of 0V.

**Table s3:** Wavelength of maximum absorption and emission ( $\lambda_{exc}=390$  nm) for compound **(3)** and compound **(4)** in different solvents

Solvent	$E_T^N$ a)	Compound <b>(3)</b>				Compound <b>(4)</b>			
		$\lambda_{abs}$ (nm)	TDDFT $\lambda_{abs}$ (nm)	$\lambda_{em}$ (nm)	$\phi_F$	$\lambda_{abs}$ (nm)	TDDFT $\lambda_{abs}$ (nm)	$\lambda_{em}$ (nm)	$\phi_F$
Chloroform	0.259	396	401.4	467		398	406.2	467	
Acetonitrile	0.460	392	401.0	462		396	403.0	468	
Ethanol	0.654	392	401.0	461	0.56 <sup>b</sup>	395	403.5	464	0.60 <sup>b</sup>

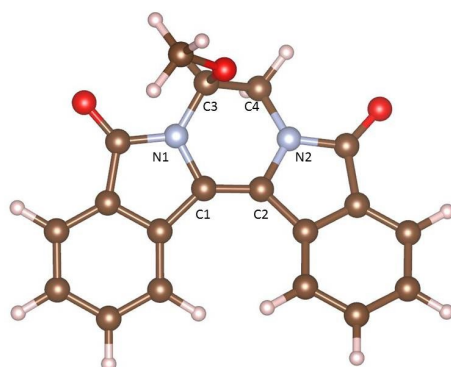
a) Normalized empirical parameters of solvent polarity.<sup>8</sup>

b) determined by the comparative method using 7-(diethylamino)-4-methylcoumarin (Coumarin 1) ( $\phi = 0.5$ ) in ethanol as reference.<sup>9</sup>

## 9. Quantum chemical calculations

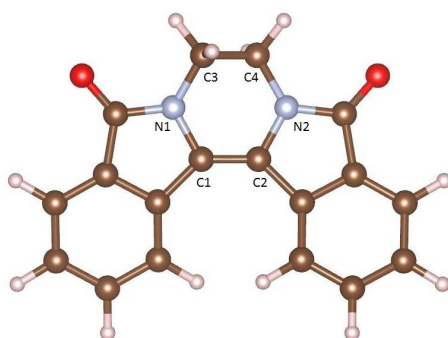
All quantum chemical calculations were performed with the Gaussian 16 software package<sup>10</sup> Geometry optimizations, followed by frequency analysis, were carried out at the B3LYP/6-31+G(d,p) theory level for compound **(3)** and **(4)** in their neutral, cationic, dicationic, anionic and dianionic forms. The frequency analysis confirmed the optimized structures as minima presenting all real valued frequencies. Solvent effects were modelled with the polarized continuum model (PCM)<sup>11,12</sup> For the TD-DFT calculations, the hybrid PBE0 functional<sup>13</sup> was used, together with the larger 6-311+G(d,p) basis set and the PCM solvent model, to take the solute into account. The equations were solved for 30 excited states.

**Table s4** - Relevant angles (degrees) and distances (Å) of compound (**3**), calculated at B3LYP/6-31+G(d,p) level in acetonitrile and the X-ray experimental structure.



	<b>N1- C1=C2-N2</b>	<b>C1=C2</b>	<b>N1-C1</b>	<b>C2-N2</b>	<b>N1-C3</b>	<b>C2-C4</b>	<b>C4-N2</b>
IMN25 <sup>2+</sup>	-23.883	1.475	1.327	1.320	1.503	1.528	1.465
IMN25 <sup>+</sup>	-15.830	1.416	1.370	1.361	1.476	1.526	1.460
IMN25	-9.231	1.367	1.416	1.410	1.458	1.525	1.454
IMN25 <sup>-</sup>	-12.410	1.403	1.419	1.411	1.449	1.527	1.451
IMN25 <sup>2-</sup>	-18.376	1.440	1.423	1.414	1.443	1.530	1.448
X-ray	-6.194	1.355	1.414	1.409	1.452	1.504	1.453

**Table s5** - Relevant angles (degrees) and distances (Å) of compound (**4**), calculated at B3LYP/6-31+G(d,p) level in acetonitrile



	<b>N1- C1=C2-N2</b>	<b>C1=C2</b>	<b>N1-C1</b>	<b>C2-N2</b>	<b>N1-C3</b>	<b>C2-C4</b>	<b>C4-N2</b>
IMN25 <sup>2+</sup>	-23.718	1.478	1.321	1.321	1.471	1.525	1.471
IMN25 <sup>+</sup>	-15.699	1.417	1.364	1.364	1.464	1.525	1.464
IMN25	-9.570	1.368	1.411	1.411	1.456	1.527	1.456
IMN25 <sup>-</sup>	-12.709	1.406	1.413	1.413	1.454	1.528	1.454
IMN25 <sup>2-</sup>	-18.425	1.442	1.417	1.417	1.450	1.531	1.450

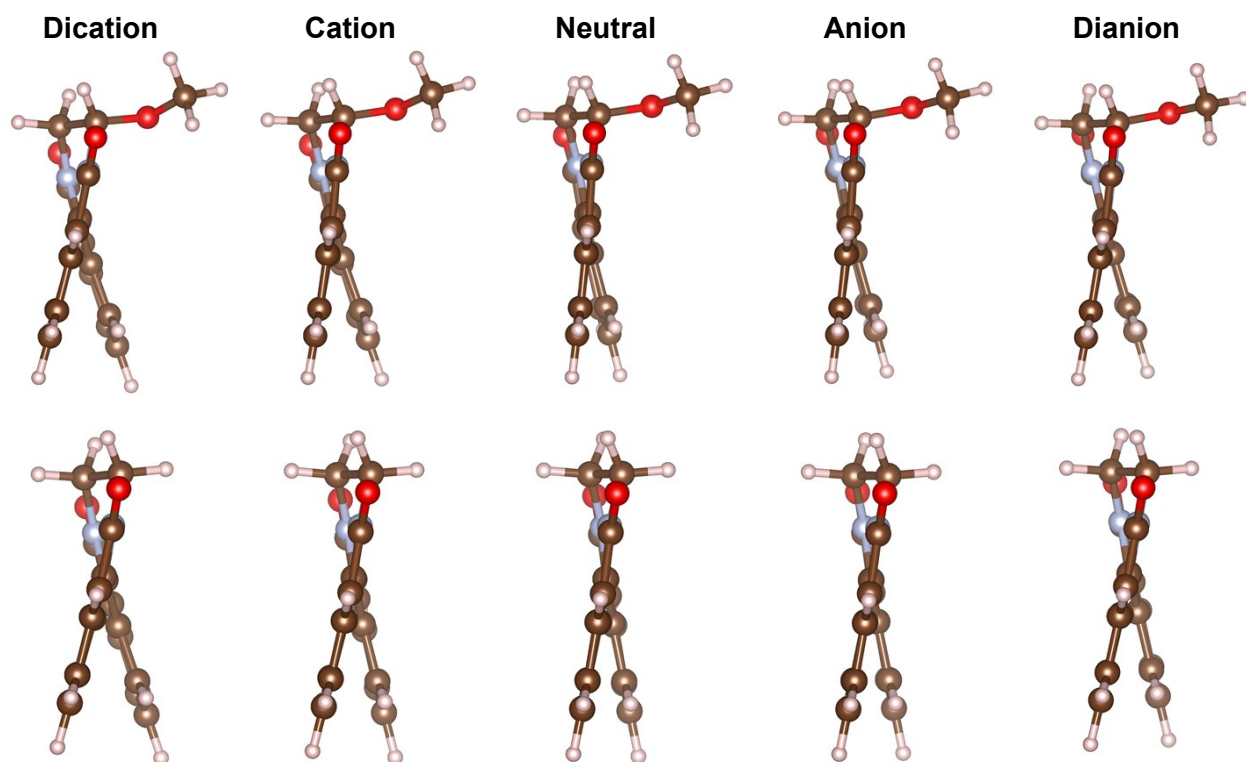


**Figure s17** – Calculated structures of compound **(3)** and related ions (top) and of compound **(4)** and related ions (bottom).

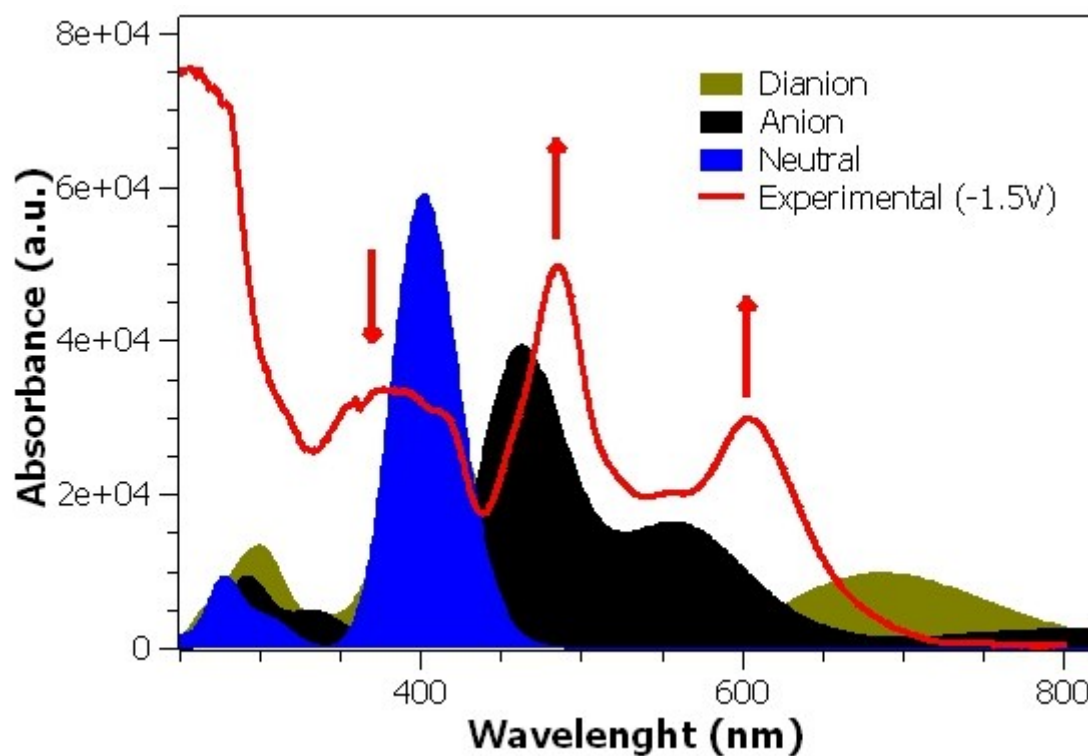


**Figure s18** – Theoretical UV/vis spectra in acetonitrile of the neutral and the negatively charged forms of compound **(3)**, calculated at PCM-pbe0/6-311+G(d,p) level, compared with an experimental spectroelectrochemistry spectra.

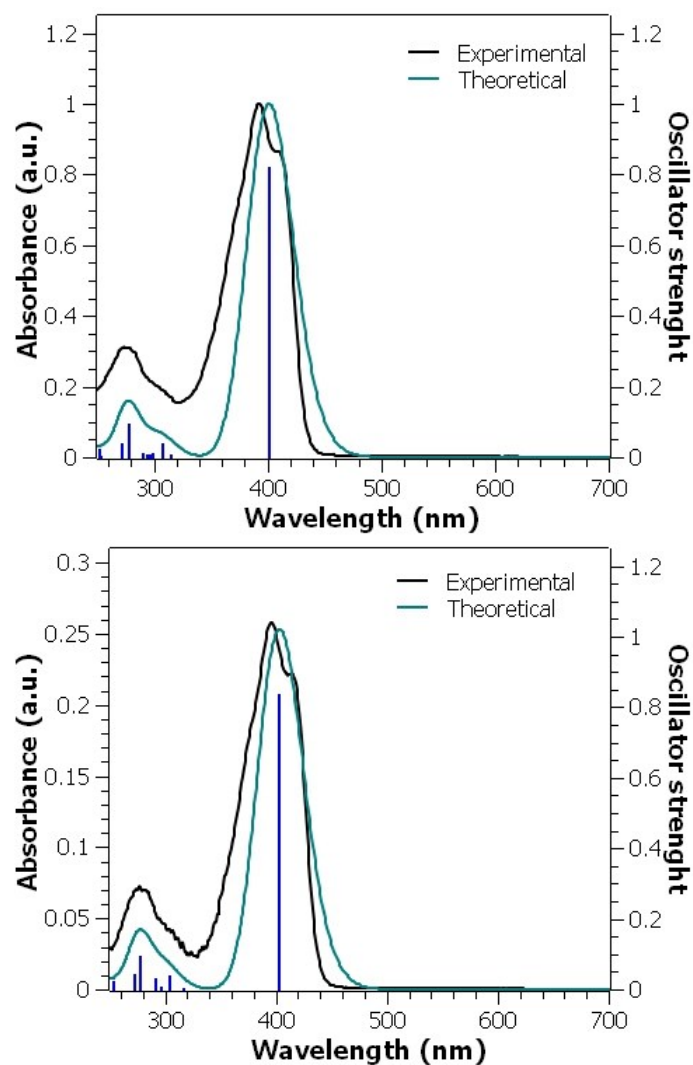


**Figure s19.** Calculated and experimental UV spectra of compound **(3)** (top) and **(4)** (bottom).

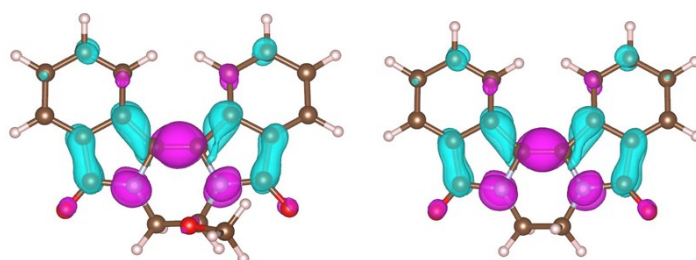


**Figure s20.** Contour plots of the electron density difference ( $\Delta\rho$ ) upon the lowest energy excitation  $S_0 \rightarrow S_1$  of the neutral compounds **(3)** (on the left) and **(4)** (on the right) in acetonitrile solution. Magenta and blue isosurfaces represent negative (loss of electrons) and positive (electron gain) values, respectively.

## 10. Hole and electron mobilities.

The electron or hole transport in an organic solid can be considered as an hopping process, that can be described by the Marcus electron transfer theory.<sup>14-17a</sup> In this theory the charge transfer rate is given by

$$k = \frac{4\pi^2}{h} V^2 (4\pi\lambda T)^{-\frac{1}{2}} \exp(-\lambda/4k_B T)$$

where  $V$  is the charge transfer matrix element,  $k_B$  is the Boltzman constant,  $h$  is the Planck constant and  $\lambda$  is the total reorganization energy. The total reorganization energy incorporates the energy change related with the geometry relaxation of molecules involved in the electron/hole transfer (inner reorganization energy,  $\lambda_{e/h}$ ) and the relaxation energy due to polarization effects in the surrounding medium (outer reorganization energy,  $\lambda_S$ ). For organic solids, the outer reorganization energy is usually much smaller than that of inner reorganization energy<sup>17b,c</sup> and total reorganization energy is then approximated by  $\lambda = \lambda_S + \lambda_{e/h} \approx \lambda_{e/h}$ . The inner reorganization energy is the required energy to adjust geometry between optimized geometries of compounds in their respective charged states and result from a sum of two components. For the hole transport,  $\lambda_h = \lambda_1 + \lambda_2$ , where the first term corresponds to the relaxation energy of the cation when it gains an electron and becomes neutral and the second term corresponds to the relaxation energy of the neutral species when it losses an electron and becomes a cation. For the electron transport process,  $\lambda_e = \lambda_3 + \lambda_4$  and the first term refers to the anion's relaxing energy when it loses an electron and becomes neutral and the second term corresponds to the neutral species' relaxing energy when it gains an electron and becomes an anion.

The mobility of a charge carrier can be calculated as <sup>(18)</sup>

$$\mu = \frac{e}{k_B T} D = \frac{e}{2dk_B T} \sum_i r_i^2 k_i p_i$$

Where  $e$  is the electron charge,  $d$  is the space dimensionality, and  $r_i$  is the hopping distance,  $k_i$  the charge transfer rate constant and  $p_i$  is the hopping probability between neighboring molecules. The hopping probability is calculated as

$$p_i = \frac{k_i}{\sum_i k_i}$$

where the sums extend over all charge hopping pathways considered, in this case the nearest neighbor molecules.

The charge transfer matrix element  $V$  can be calculated by the Koopmans' theorem method <sup>(19)</sup>

$$V = \frac{E_{Homo/Lumo+1} - E_{Homo-1/Lumo}}{2}$$

where  $E$  is the energy of the HOMO, HOMO-1, LUMO and LUMO+1 levels of the neutral adjacent molecular pairs. For this calculation, the PW91PW91 functional, which had presented a good performance in previous studies <sup>(20),(21)(22)</sup> was employed, with the 6-31+g(d,p) basis set.

The carrier mobilities calculated for compound **(3)** are presented in table **s5** and comparable with experimental results of other imide type materials (see the discussion on the state of the art in the main paper). As both the electron and hole mobilities are of similar magnitude an the ambipolar charge transport characteristics of this compound is to be expected although with a tendency towards n-type material.

A further estimation can be performed, assuming the same value of  $V$  <sup>(23)</sup>. With this assumption, for a given temperature, the  $k_h/k_e$  ratio calculated allows one to compare the electron and hole mobilities. The results show that the compounds **(3)** and **(4)** are essentially electron transport compounds.

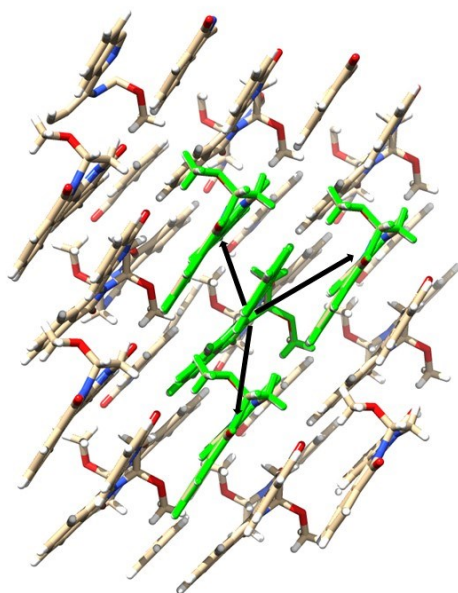


**Figure s21.** Charge hopping pathways schemes for compound **(3)** crystals.

**Table s6.** Calculated reorganization energies ( $\lambda_h$  and  $\lambda_e$ ) and its components ( $\lambda_1$ ,  $\lambda_2$ ,  $\lambda_3$  and  $\lambda_4$ ) (in eV) at the b3lyp/6-31+g(d,p) level. Relative hoping rates of electrons versus holes ( $k_e/k_h$ ) calculated at 300K. Calculated carrier mobilities (in  $\text{cm}^2\text{V}^{-1}\text{s}^{-1}$ ) for compound **(3)**

	$\lambda_1$	$\lambda_2$	$\lambda_h$	$\lambda_3$	$\lambda_4$	$\lambda_e$	$k_e/k_h$	$\mu_-$	$\mu_+$
<b>3</b>	0.219	0.234	0.453	0.191	0.190	0.380	2.201	0.731	0.379
<b>4</b>	0.205	0.217	0.421	0.184	0.180	0.364	1.882	-	-

**11. Calculated absorption data for compounds (3) and (4) and the main-orbitals involved in the transitions.**

**Compound 3<sup>2</sup>**

**Table s7**

<b>State</b>	$\lambda$ (nm)	$f$	<b>Major MO <math>\rightarrow</math> MO transitions</b>
S <sub>1</sub>	623.4	0.018	HOMO $\rightarrow$ LUMO (93%)
S <sub>2</sub>	603.1	0.036	H-1 $\rightarrow$ LUMO (87%)
S <sub>3</sub>	552.9	0.022	H-4 $\rightarrow$ LUMO (31%), H-3 $\rightarrow$ LUMO (37%), H-2 $\rightarrow$ LUMO (29%)
S <sub>4</sub>	522.0	0.096	H-3 $\rightarrow$ LUMO (38%), H-2 $\rightarrow$ LUMO (51%)
S <sub>5</sub>	483.0	0.115	H-4 $\rightarrow$ LUMO (58%), H-3 $\rightarrow$ LUMO (16%), H-2 $\rightarrow$ LUMO (13%)
S <sub>6</sub>	450.2	0.003	H-5 $\rightarrow$ LUMO (90%)
S <sub>7</sub>	435.9	0.001	H-6 $\rightarrow$ LUMO (89%)
S <sub>8</sub>	346.0	0.016	H-7 $\rightarrow$ LUMO (97%)
S <sub>9</sub>	328.8	0.020	HOMO $\rightarrow$ L+1 (96%)
S <sub>10</sub>	321.1	0.006	H-1 $\rightarrow$ L+1 (96%)

**Compound 3<sup>+</sup>**

**Table s8**

<b>State</b>	$\lambda$ (nm)	$f$	<b>Major MO <math>\rightarrow</math> MO transitions</b>
S <sub>1</sub>	674.4	0.008	HOMO( $\beta$ ) $\rightarrow$ LUMO( $\beta$ ) (89%)
S <sub>2</sub>	642.7	0.012	H-1( $\beta$ ) $\rightarrow$ LUMO( $\beta$ ) (88%)

S <sub>3</sub>	570.2	0.038	H-2( $\beta$ )->LUMO( $\beta$ ) (87%)
S <sub>4</sub>	565.6	0.046	H-3( $\beta$ )->LUMO( $\beta$ ) (87%)
S <sub>5</sub>	527.2	0.016	H-6( $\beta$ )->LUMO( $\beta$ ) (19%), H-4( $\beta$ )->LUMO( $\beta$ ) (66%)
S <sub>6</sub>	516.3	0.258	HOMO( $\alpha$ )->LUMO( $\alpha$ ) (83%)
S <sub>7</sub>	506.6	0.012	H-5( $\beta$ )->LUMO( $\beta$ ) (86%)
S <sub>8</sub>	453.5	0.002	H-6( $\beta$ )->LUMO( $\beta$ ) (69%), H-4( $\beta$ )->LUMO( $\beta$ ) (24%)
S <sub>9</sub>	388.8	0.018	H-1( $\alpha$ )->LUMO( $\alpha$ ) (50%), HOMO( $\beta$ )->L+1( $\beta$ ) (13%)
S <sub>10</sub>	379.1	0.031	H-2( $\alpha$ )->LUMO( $\alpha$ ) (45%), H-1( $\beta$ )->L+1( $\beta$ ) (12%)

### Compound 3

Table s9

State	$\lambda$ (nm)	$f$	Major MO $\rightarrow$ MO transitions
S <sub>1</sub>	401.0	0.817	HOMO->LUMO (99%)
S <sub>2</sub>	315.3	0.003	H-1->LUMO (30%), HOMO->L+1 (62%), H-2->LUMO (4%)
S <sub>3</sub>	307.8	0.034	H-1->LUMO (60%), HOMO->L+1 (23%), H-2->LUMO (4%), HOMO->L+2 (4%)
S <sub>4</sub>	299.9	0.010	H-5->LUMO (10%), H-2->LUMO (49%), HOMO->L+2 (22%), H-4->LUMO (4%), H-3->LUMO (3%), HOMO->L+1 (5%)
S <sub>5</sub>	296.4	0.004	H-5->LUMO (52%), H-4->LUMO (18%), H-7->LUMO (3%), H-6->LUMO (5%), H-6->L+1 (2%), H-2->LUMO (9%), HOMO->L+2 (7%)
S <sub>6</sub>	294.5	0.004	H-4->LUMO (12%), H-2->LUMO (25%), HOMO->L+2 (50%), H-6->LUMO (9%)
S <sub>7</sub>	291.0	0.008	H-6->LUMO (73%), H-7->LUMO (3%), H-5->LUMO (3%), H-2->LUMO (3%), H-1->LUMO (3%), HOMO->L+2 (7%)
S <sub>8</sub>	278.0	0.092	H-3->LUMO (82%), H-1->L+2 (3%), HOMO->L+1 (6%)
S <sub>9</sub>	272.8	0.036	H-5->LUMO (21%), H-4->LUMO (56%), H-2->LUMO (3%), HOMO->L+2 (9%)
S <sub>10</sub>	253.8	0.002	H-7->LUMO (84%), H-5->LUMO (4%), HOMO->L+3 (4%)

### Compound 3

Table s10

State	$\lambda$ (nm)	$f$	Major MO $\rightarrow$ MO transitions
S <sub>1</sub>	813.9	0.034	HOMO( $\alpha$ )->LUMO( $\alpha$ ) (91%)
S <sub>2</sub>	688.1	0.006	HOMO( $\alpha$ )->L+1( $\alpha$ ) (94%)
S <sub>3</sub>	560.7	0.220	HOMO( $\alpha$ )->L+2( $\alpha$ ) (14%), HOMO( $\beta$ )->LUMO( $\beta$ ) (77%)
S <sub>4</sub>	462.2	0.542	HOMO( $\alpha$ )->L+2( $\alpha$ ) (82%), HOMO( $\beta$ )->LUMO( $\beta$ ) (13%)
S <sub>5</sub>	413.5	0.001	HOMO( $\alpha$ )->L+3( $\alpha$ ) (96%)
S <sub>6</sub>	385.4	0.005	H-1( $\alpha$ )->LUMO( $\alpha$ ) (22%), HOMO( $\beta$ )->L+1( $\beta$ ) (61%)
S <sub>7</sub>	371.0	0.000	H-1( $\alpha$ )->L+1( $\alpha$ ) (11%), H-1( $\beta$ )->LUMO( $\beta$ ) (18%), HOMO( $\beta$ )->L+2( $\beta$ ) (37%)
S <sub>8</sub>	365.5	0.001	HOMO( $\alpha$ )->L+4( $\alpha$ ) (82%), HOMO( $\alpha$ )->L+5( $\alpha$ ) (14%)
S <sub>9</sub>	358.9	0.001	HOMO( $\alpha$ )->L+4( $\alpha$ ) (14%), HOMO( $\alpha$ )->L+5( $\alpha$ ) (79%)
S <sub>10</sub>	356.5	0.009	H-2( $\beta$ )->LUMO( $\beta$ ) (11%), H-1( $\beta$ )->LUMO( $\beta$ ) (40%)

### Compound 3<sup>2-</sup>

Table s11

State	$\lambda$ (nm)	$f$	Major MO $\rightarrow$ MO transitions
S <sub>1</sub>	692.8	0.121	HOMO->LUMO (98%)
S <sub>2</sub>	635.8	0.023	HOMO->L+1 (99%)
S <sub>3</sub>	505.7	0.000	HOMO->L+2 (97%)
S <sub>4</sub>	440.7	0.005	HOMO->L+3 (85%), HOMO->L+4 (10%)
S <sub>5</sub>	431.5	0.015	HOMO->L+3 (11%), HOMO->L+4 (86%)
S <sub>6</sub>	416.3	0.350	HOMO->L+5 (92%)
S <sub>7</sub>	387.8	0.192	HOMO->L+6 (91%)
S <sub>8</sub>	382.6	0.005	HOMO->L+7 (89%)
S <sub>9</sub>	375.9	0.010	HOMO->L+8 (90%)
S <sub>10</sub>	369.0	0.003	HOMO->L+9 (86%)

### Compound 4<sup>2+</sup>

Table s12

State	$\lambda$ (nm)	$f$	Major MO $\rightarrow$ MO transitions
S <sub>1</sub>	617.7	0.040	HOMO->LUMO (92%)
S <sub>2</sub>	589.2	0.002	H-1->LUMO (97%)

S <sub>3</sub>	518.4	0.084	H-2->LUMO (92%)
S <sub>4</sub>	489.4	0.138	H-3->LUMO (97%)
S <sub>5</sub>	453.8	0.001	H-4->LUMO (94%)
S <sub>6</sub>	439.3	0.000	H-5->LUMO (93%)
S <sub>7</sub>	326.5	0.005	HOMO->L+1 (96%)
S <sub>8</sub>	318.4	0.003	H-1->L+1 (86%)
S <sub>9</sub>	305.7	0.194	H-6->LUMO (68%), H-3->L+1 (28%)
S <sub>10</sub>	298.8	0.117	H-2->L+1 (93%)

### Compound 4<sup>+</sup>

Table s13

State	$\lambda$ (nm)	<i>f</i>	Major MO $\rightarrow$ MO transitions
S <sub>1</sub>	686.6	0.003	HOMO( $\beta$ )->LUMO( $\beta$ ) (93%)
S <sub>2</sub>	633.8	0.010	H-1( $\beta$ )->LUMO( $\beta$ ) (92%)
S <sub>3</sub>	561.9	0.045	H-2( $\beta$ )->LUMO( $\beta$ ) (89%)
S <sub>4</sub>	551.5	0.054	H-3( $\beta$ )->LUMO( $\beta$ ) (93%)
S <sub>5</sub>	515.9	0.257	HOMO( $\alpha$ )->LUMO( $\alpha$ ) (88%)
S <sub>6</sub>	505.6	0.000	H-4( $\beta$ )->LUMO( $\beta$ ) (90%)
S <sub>7</sub>	503.2	0.006	H-5( $\beta$ )->LUMO( $\beta$ ) (88%)
S <sub>8</sub>	388.7	0.002	H-1( $\alpha$ )->LUMO( $\alpha$ ) (55%), HOMO( $\beta$ )->L+1( $\beta$ ) (15%)
S <sub>9</sub>	385.5	0.116	H-2( $\alpha$ )->LUMO( $\alpha$ ) (41%), H-6( $\beta$ )->LUMO( $\beta$ ) (21%), H-1( $\beta$ )->L+1( $\beta$ ) (11%)
S <sub>10</sub>	361.9	0.203	H-6( $\beta$ )->LUMO( $\beta$ ) (67%)

### Compound 4

Table s14

State	$\lambda$ (nm)	<i>f</i>	Major MO $\rightarrow$ MO transitions
S <sub>1</sub>	403.0	0.834	HOMO->LUMO (99%)
S <sub>2</sub>	317.2	0.002	H-1->LUMO (63%), HOMO->L+1 (34%)
S <sub>3</sub>	308.2	0.000	H-1->LUMO (33%), HOMO->L+1 (58%), H-3->LUMO (4%)
S <sub>4</sub>	303.9	0.036	H-2->LUMO (59%), HOMO->L+2 (30%), H-5->LUMO (9%)
S <sub>5</sub>	297.2	0.004	H-5->LUMO (28%), HOMO->L+2 (55%), H-4->LUMO

			(4%), H-2->LUMO (9%)
S <sub>6</sub>	291.2	0.030	H-5->LUMO (54%), H-2->LUMO (24%), H-6->L+1 (2%), H-4->LUMO (9%), HOMO->L+2 (7%)
S <sub>7</sub>	291.1	0.000	H-6->LUMO (90%), H-5->L+1 (5%)
S <sub>8</sub>	277.2	0.090	H-3->LUMO (84%), H-2->L+1 (3%), H-1->L+2 (3%), HOMO->L+1 (6%)
S <sub>9</sub>	273.0	0.038	H-4->LUMO (76%), H-2->LUMO (5%), H-2->L+2 (4%), H-1->L+1 (5%), HOMO->L+2 (7%)
S <sub>10</sub>	254.2	0.021	HOMO->L+3 (87%), H-2->L+1 (4%), H-1->L+2 (5%)

### Compound 4<sup>-</sup>

Table s15

State	$\lambda$ (nm)	<i>f</i>	Major MO $\rightarrow$ MO transitions
S <sub>1</sub>	797.7	0.030	HOMO( $\alpha$ )->LUMO( $\alpha$ ) (91%)
S <sub>2</sub>	689.7	0.006	HOMO( $\alpha$ )->L+1( $\alpha$ ) (94%)
S <sub>3</sub>	562.9	0.217	HOMO( $\alpha$ )->L+2( $\alpha$ ) (15%), HOMO( $\beta$ )->LUMO( $\beta$ ) (76%)
S <sub>4</sub>	464.0	0.563	HOMO( $\alpha$ )->L+2( $\alpha$ ) (82%), HOMO( $\beta$ )->LUMO( $\beta$ ) (14%)
S <sub>5</sub>	419.8	0.000	HOMO( $\alpha$ )->L+3( $\alpha\alpha$ ) (95%)
S <sub>6</sub>	384.7	0.004	H-1( $\alpha$ )->LUMO( $\alpha$ ) (19%), HOMO( $\beta$ )->L+1( $\beta$ ) (56%)
S <sub>7</sub>	371.7	0.001	H-1( $\alpha$ )->L+1( $\alpha$ ) (12%), H-2( $\beta$ )->LUMO( $\beta$ ) (18%), HOMO( $\beta$ )->L+2( $\beta$ ) (43%)
S <sub>8</sub>	367.0	0.001	HOMO( $\alpha$ )->L+4( $\alpha$ ) (95%)
S <sub>9</sub>	362.6	0.000	HOMO( $\alpha$ )->L+5( $\alpha$ ) (92%)
S <sub>10</sub>	359.9	0.008	H-1( $\beta$ )->LUMO( $\beta$ ) (57%)

### Compound 4<sup>2-</sup>

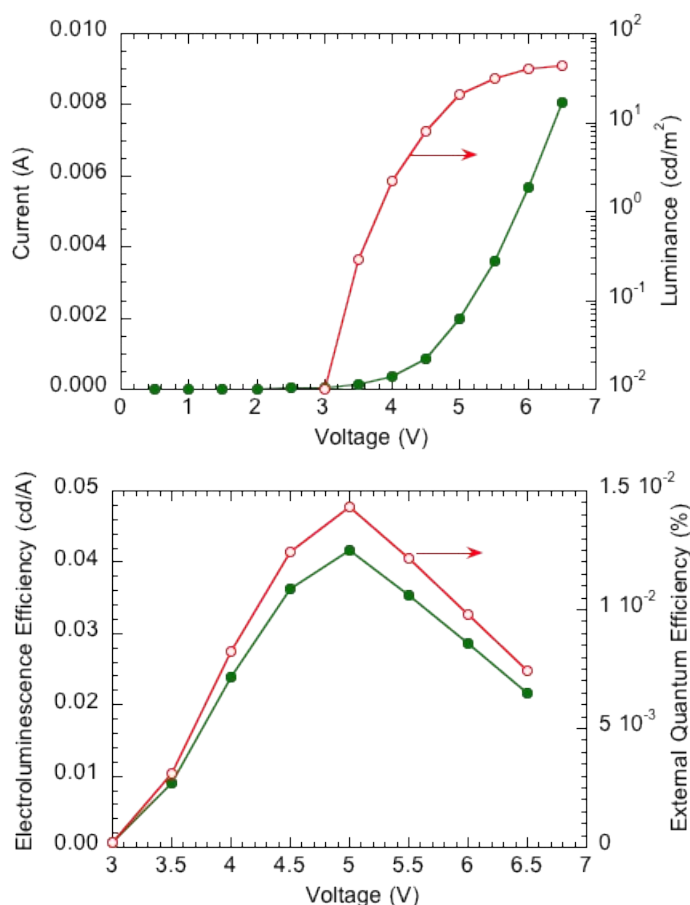
Table s16

State	$\lambda$ (nm)	<i>f</i>	Major MO $\rightarrow$ MO transitions
S <sub>1</sub>	1047.3	0.020	HOMO->LUMO (96%)
S <sub>2</sub>	924.4	0.003	H-1->LUMO (98%)
S <sub>3</sub>	666.3	0.001	H-4->LUMO (93%)
S <sub>4</sub>	663.4	0.009	H-5->LUMO (80%), H-2->LUMO (14%)
S <sub>5</sub>	646.5	0.046	H-5->LUMO (14%), H-2->LUMO (83%)

S <sub>6</sub>	594.9	0.132	H-3->LUMO (97%)
S <sub>7</sub>	410.6	0.001	HOMO->L+1 (97%)
S <sub>8</sub>	397.7	0.342	H-6->LUMO (83%), H-1->L+1 (15%)
S <sub>9</sub>	385.9	0.120	H-6->LUMO (14%), H-1->L+1 (80%)
S <sub>10</sub>	341.4	0.000	H-7->LUMO (95%)

## 12. Electroluminescence studies

Light-emitting diodes were prepared on glass/ITO substrates (ITO = indium-tin oxide), which were cleaned with detergent, distilled water, acetone and isopropanol. They were treated with oxygen plasma prior to the deposition of PEDOT:PSS (poly(3,4-ethylenedioxythiophene) doped with polystyrene sulfonic acid, CLEVIOS P VP.AI 4083 from Heraeus Clevios GmbH) by spin coating. The PEDOT:PSS films (75 nm thick, as measured with a DEKTAK profilometer) were annealed in air for 10 minutes at 120 °C. Films of compound (**3**), with a thicknesses of 75 nm, were deposited on top of PEDOT:PSS by spin coating, from a chloroform solution. The substrates were then placed inside an evaporation chamber to deposit the top cathodes, which consisted of calcium (20 nm) protected with an overlayer of aluminium (75 nm thick). Deposition was made at a base pressure of  $2 \times 10^{-6}$  mbar through a shadow mask, defining pixel areas of 4 mm<sup>2</sup>. Devices were tested under vacuum using a K2400 Source Meter and a calibrated silicon photodiode, as described previously.<sup>24</sup> The electroluminescence (EL) spectra were obtained with a CCD spectrograph (from ScanSci). External quantum efficiency values were estimated as detailed in ref. 24.



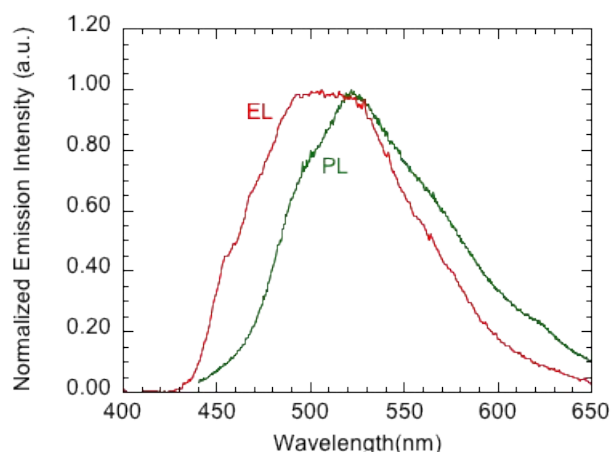


**Figure s22.** Performance of an OLED based on compound **(3)** having the structure ITO/PEDOT:PSS/(**3**)/Ca/Al.

An extensive study of the stability of films of compounds **(3)** and **(4)** was carried out as this is relevant for applications and also to direct future molecular structure modifications. Despite the stability studies performed above (section 4.3) and the fact that these compounds can be left in the open air for several days, without any structural changes, these studies in films indicated that there was certain changes occurring upon exposure to ambient atmosphere, as observed by the evolution of the optical absorption of thin films deposited by spin coating, inside a glove box on spectroil discs. Figure s22 shows a typical result found for a film of compound **(3)**, where the absorption spectrum was recorded as a function of the environmental exposure time. A similar bleaching occurs when the films are kept in air in the dark.

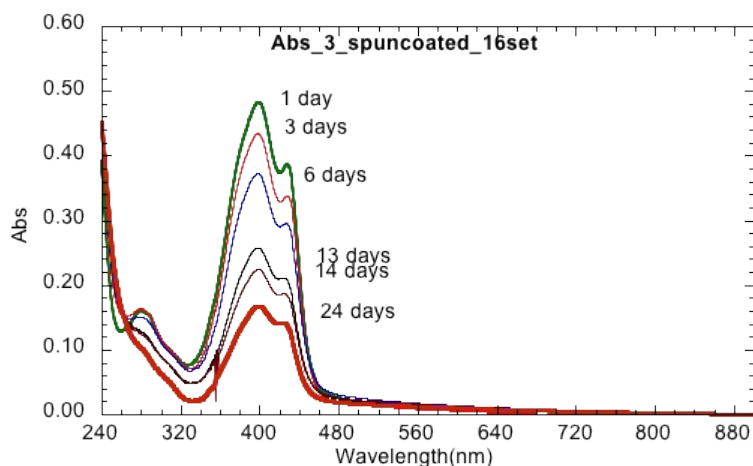


**Figure s23.** Evolution of the absorption spectrum of a thin film of **(3)** as a function of environmental exposure time. Upon normalization of the absorption spectra, we find that there is an almost perfect overlap of the main absorption band.

Despite the observations for the bulk compound given above and the experiments carried out in section 4, in the film state, it seems that this bleaching is the result of oxidation of the compound by atmospheric oxygen.

Two thin films of compound **(3)** were also prepared by sublimation using the thermal evaporator inserted in the glove box. The stability of the two films was also followed by UV/Vis absorption, up to 28 days, as shown in Figure s15. As found for spin coated films, the environmental exposure leads to the thin film bleaching, an effect that is almost negligible when the sample is kept inside the glove box.

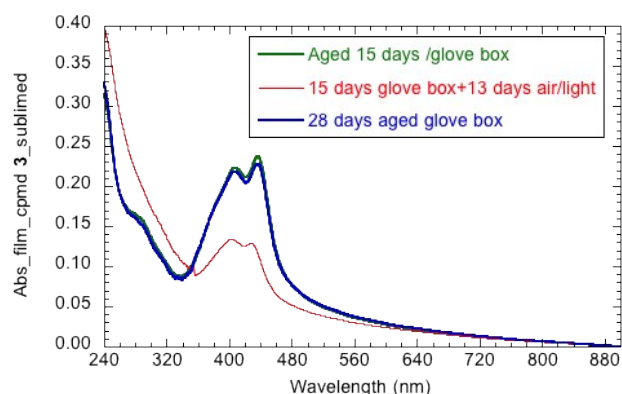


**Figure s24.** Variation of the UV/Vis absorption spectra of two sublimed films, depending on the aging conditions.

It is also worth pointing out that compound (**3**) thin films are amorphous after preparation, as assessed by their transparency, but tend to crystallize over time. This is, however, a process whose kinetics is not well-defined, as the time it takes to be visible varies significantly from film to film. This is not unexpected as the crystallization process is controlled by a nucleation process. Figure s24 compares two films deposited on glass/ITO/PEDOT:PSS substrates, later used to fabricate LEDs, aged for 35 h inside of the glove box and in air/dark, evidencing the variation of the crystallization process kinetics.

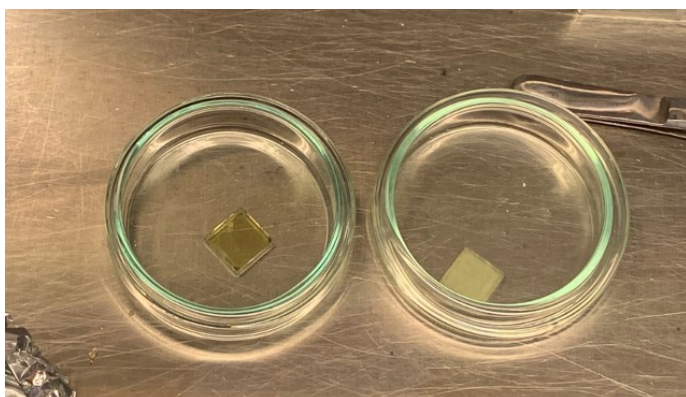


**Figure s25.** Films of (**3**) deposited by spin coating in ITO/PEDOT:PSS and aged for 35h inside the glove box (substrate on the left) and in air/dark (substrate on the right).

The extent of aging influences the performance of the LEDs. Aging of the films, prior to the deposition of the top metal electrodes, up to 2 days, either inside or outside the glove box does not have a significant detrimental effect. A 5-day aging period has little effect on the LEDs performance, if the aging is carried out inside the glove box, but has a significant detrimental effect when the glass/ITO/PEDOT:PSS/(**3**) substrates are aged in air/dark, as shown in Figure s24. The emission spectra of these LEDs does not change (in the case of the LED prepared with the film aged for 5 days in air/dark the emission was too weak to allow a recording of the emission spectrum).

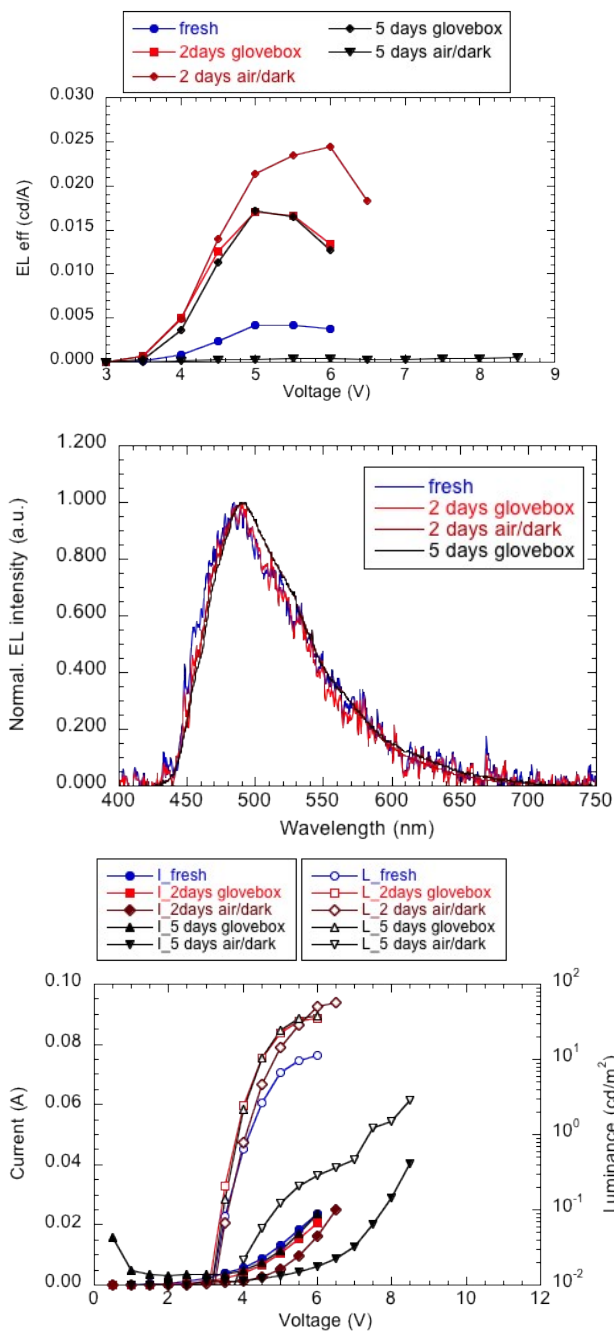


**Figure s26.** Effect of aging on the performance of LEDs with structure ITO/PEDOT:PSS/(3)/Ca/Al structure.

Compound (4) shows a similar behaviour. However, the crystallization has a faster kinetics, as the films prepared by spin coating right after drying show crystallization signs (poor transparency and long tail in the absorption spectrum). This is shown in Figure S26. In this case it appears as if compound aging inside the glove box induced some bleaching of the film. This is quite surprising and requires further studies in the future.

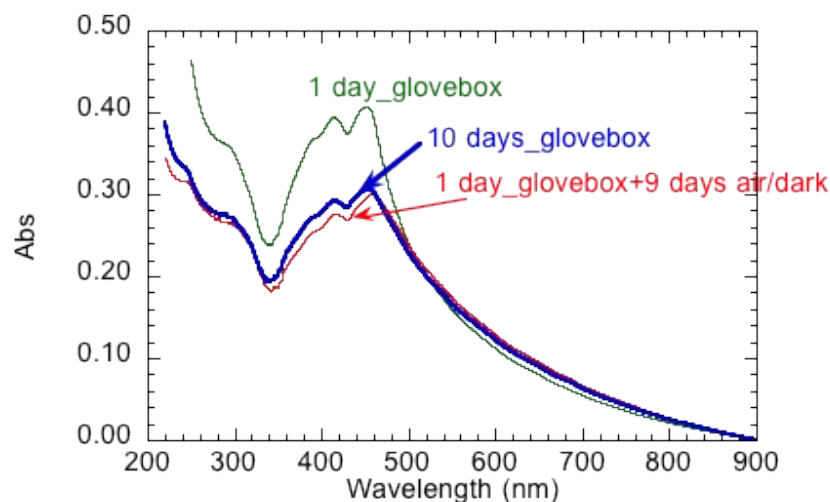


**Figure s27.** Variation of the absorption spectrum of a thin film of (4) on Spectrosil upon aging.

## 12. References

- (1) W. Perrin, *Purification of Laboratory Chemicals*, fourth ed., Butterworth Heinemann, Oxford, **1996**.
- (2) C. S. Marques, D. Peixoto, A. J. Burke, *RSC Adv.* **2015**, 5, 20108-20114.
- (3) J. Sun, Y. Dong, L. Cao, X. Wang, S. Wang, Y. Hu, *J. Org. Chem.* **2004**, 69, 8932-8934.
- (4) a) D. Solé, F. Mariani, I. Fernández, M. A. Sierra, *J. Org. Chem.* **2012**, 77, 10272. b) D. Solé, F. Mariani, I. Fernández, *Adv. Synth. Catal.* **2014**, 356, 3237.
- (5) S. Mann, L. Eveleigh, O. Lequin, O. Ploux, *Analytical Biochem.* **2013**, 432, 90-96.
- (6) a) S. Zhou, E. Doni, G. M. Anderson, R. G. Kane, S.W. MacDougall, V. M. Ironmonger, T. Tuttle, J. A. Murphy, *J. Am. Chem. Soc.* **2014**, 136, 17818-17826. b) T. Krchová, J. Kotek, D. Jiráček, J. Havlíčková, I. Císařová, P. Hermann, *Dalton Trans.*, **2013**, 42, 15735-15747.
- (7) X.-F. Duan, J. Zeng, J.-W. Lu, Z.-B. Zhang, *J. Org. Chem.* **2006**, 71, 9873-9876.
- (8) C. Reichardt, *Solvents and Solvent Effects in Organic Chemistry*, 3<sup>rd</sup> Edition; Wiley-VCH Verlag GmbH & Co. KGaA, Weinheim, **2003**.
- (9) M. Taniguchi, J.S. Lindsey, *Photochem. Photobiol.* **2018**, 94, 290.
- (10) Gaussian 16, Revision B.01, M. J. Frisch, G. W. Trucks, H. B. Schlegel, G. E. Scuseria, M. A. Robb, J. R. Cheeseman, G. Scalmani, V. Barone, G. A. Petersson, H. Nakatsuji, X. Li, M. Caricato, A. V. Marenich, J. Bloino, B. G. Janesko, R. Gomperts, B. Mennucci, H. P. Hratchian, J. V. Ortiz, A. F. Izmaylov, J. L. Sonnenberg, D. Williams-Young, F. Ding, F. Lipparini, F. Egidi, J. Goings, B. Peng, A. Petrone, T. Henderson, D. Ranasinghe, V. G. Zakrzewski, J. Gao, N. Rega, G. Zheng, W. Liang, M. Hada, M. Ehara, K. Toyota, R. Fukuda, J. Hasegawa, M. Ishida, T. Nakajima, Y. Honda, O. Kitao, H. Nakai, T. Vreven, K. Throssell, J. A. Montgomery, Jr., J. E. Peralta, F. Ogliaro, M. J. Bearpark, J. J. Heyd, E. N. Brothers, K. N. Kudin, V. N. Staroverov, T. A. Keith, R. Kobayashi, J. Normand, K. Raghavachari, A. P. Rendell, J. C. Burant, S. S. Iyengar, J. Tomasi, M. Cossi, J. M. Millam, M.

- Klene, C. Adamo, R. Cammi, J. W. Ochterski, R. L. Martin, K. Morokuma, O. Farkas, J. B. Foresman, D. J. Fox, Gaussian, Inc., Wallingford CT, **2016**.
- (11) C. Amovilli, V. Barone, R. Cammi, E. Cancès, M. Cossi, B. Mennucci, C. S. Pomelli, J. Tomasi, *J. Adv. Quantum Chem.*, **1998**, 32, 227–261.
- (12) M. Cossi, V. Barone, *J. Chem. Phys.*, **2001**, 115, 4708.
- (13) C. Adamo and V. Barone, *J. Chem. Phys.*, **1999**, 110, 6158.
- (14) Marcus, R. A. *J. Chem. Phys.* **1956**, 24, 966.
- (15) Marcus, R. A. *J. Chem. Phys.* **1965**, 43, 679.
- (16) Newton, M. D.; Sutin, N. *Annual Rev. Phys. Chem.* **1984**, 35, 437.
- (17) a) Barbara, P. F.; Meyer, T. J.; Ratner, M. A. *J. Phys. Chem.* **1996**, 100, 13148; b) S. Di Motta, E. Di Donato, F. Negri, G. Orlandi, D. Fazzi and C. Castiglioni, *Journal of the American Chemical Society*, 2009, 131, 6591-6598. c) D. McMahon and A. Troisi, *The Journal of Physical Chemistry Letters*, 2010, 1, 941-946.
- (18) Deng, W. Q.; Goddard, W. A. *J. Phys. Chem. B* 2004, 108, 8614.
- (19) S. -Z. Lu, X. -Y. Li, and J. -F. Liu, *J. Phys. Chem. A* **2004** 108 (18), 4125-4131
- (20) G. Nan, X. Yang, L. Wang, Z. Shuai, and Y. Zhao *Phys. Rev. B* **2009**, 79, 115203
- (21) X. Yang, L. Wang, C. Wang, W. Long, and Z. Shuai *Chem. Mater.* **2008** 20 (9), 3205-3211
- (22) Chen, Z., Li, Y., He, Z., Xu, Y., & Yu, W. *Journal of Chemical Research*, **2019** 43(7–8), 293–303.
- (23) Lin, B. C., Cheng, C. P., & Lao, Z. P. M. *J. Phys Chem. A* **2003**, 107(26).
- (24) Morgado, A. Charas, J. A. Fernandes, I. S. Gonçalves, L. D. Carlos and L. Alcácer, *J. Phys. D: Appl. Phys.* **2006**, 39, 3582.